2013

Assimilation of Lightning Data Using a Nudging Method Involving Low-Level Warming

Max R. Marchand

THE FLORIDA STATE UNIVERSITY

COLLEGE OF ARTS AND SCIENCES

ASSIMILATION OF LIGHTNING DATA USING A NUDGING METHOD INVOLVING LOW-LEVEL WARMING

By

MAX R. MARCHAND

A Thesis submitted to the
Department of Earth, Atmospheric, and Ocean Sciences
in partial fulfillment of the
requirements for the degree of
Master of Science

Degree Awarded:
Summer Semester, 2013

Max Marchand defended this thesis on May 28, 2013.
The members of the supervisory committee were:

Henry Fuelberg
Professor Directing Thesis

Jon Ahlquist
Committee Member

Robert Hart
Committee Member

The Graduate School has verified and approved the above-named committee members, and certifies that the thesis has been approved in accordance with university requirements.

ACKNOWLEDGMENTS

Acknowledgement must be given foremost to my advisor Dr. Henry Fuelberg. Dr. Fuelberg was tremendously helpful in guiding me through this research and motivating me to contemplate every section and sentence of this thesis and to write with the best of my ability. I am deeply appreciative of him giving me the opportunity to work on this intriguing, yet challenging research subject the past three years. I also must acknowledge and express appreciation for the knowledge Dr. I. Michael Navon and Dr. Razvan Stefanescu have imparted on me about data assimilation while collaborating on this subject. Without this knowledge it is unlikely I would have had the confidence to pursue the thesis topic that I did. Gratitude is also given for the funding of this research provided by NOAA Grant NA10NES4400008 under the auspices of the Joint Center for Satellite Data Assimilation. I also am thankful for the gracious input offered by my committee members, Drs. Jon Ahlquist and Robert Hart.

Additionally, I would like to thank past and present members of the Fuelberg Lab as much aid has been given in computing and research concerns. I also thank the Fuelberg Lab for testing and strengthening my poise and composure every day I was in the Lab. Eventually with these new found qualities of discipline and focus, the 12-hour work days imperative to the completion of this thesis became manageable. I also must acknowledge my parents for their financial support and, along with my brother and sister, for cultivating my interests and thirst for ever more knowledge and understanding.

TABLE OF CONTENTS

LIST OF FIGURES

LIST OF ACRONYMS

3DVAR	three-dimensional variational analysis
4DVAR	four-dimensional variational analysis
BIA	bias score or frequency bias
BMJ	Betts-Miller-Janjic cumulus parameterization scheme
CAPE	convective available potential energy
CCL	convective condensation level
CPS	cumulus parameterization scheme
CT	simulation not employing lightning data assimilation
EnKF	ensemble Kalman filter
ENTLN	Earth Networks Total Lightning Network
ETS	equitable threat score
FDDA	four-dimensional data assimilation
FNL	NCEP Final Operational Global Analysis
FO	lightning data assimilation method from Fierro et al. (2012)
FO24	simulation employing FO method for entire 24 h period
FSS	fractions skill score
GLM	Geostationary Lightning Mapper
KF	Kain-Fritsch cumulus parameterization scheme
LFC	level of free convection
MU	our lightning data assimilation method warming the most unstable levels
MU24	simulation employing MU method for entire 24 h period
MUL	most unstable level
POFD	probability of false detection
PW	precipitable water
qgmax	maximum graupel mixing ratio in a grid column
ST4	NCEP stage IV hourly precipitation observations
WRF	Weather Research and Forecasting Model

ABSTRACT

This study presents a new method for assimilating lightning data into numerical models that is suitable for cloud-resolving scales (e.g., 3 km). The study utilized data from the Earth Networks Total Lightning Network at 9 km grid spacing to mimic the resolution of the Geostationary Lightning Mapper (GLM) that will be on the upcoming GOES-R satellites. The assimilation procedure was developed using the Weather Research and Forecasting (WRF) numerical model. The method (denoted MU) warms the most unstable low levels of the atmosphere at locations where lightning was observed but deep convection was not simulated based on the absence of graupel. Simulation results utilizing the new method are compared with a control simulation and a simulation employing the lightning assimilation method (FO) developed by Alexandre Fierro and colleagues. Unlike MU, the FO method increases relative humidity according to a nudging function dependent on the intensity of observed lightning and simulated graupel mixing ratio. Simulations are performed across the Central and Eastern United States for three separate severe storm cases during 2011. These cases exhibit a wide range of weather patterns and thunderstorm organization. When comparing simulation results with hourly NCEP stage IV radar and gauge precipitation observations, both the MU and FO assimilation methods produce an improved simulated precipitation field during the assimilation period and a short time afterwards based on subjective comparison and objective statistical scores. The assimilation methods commonly improve equitable threat scores by more than 0.1 and 50% during the assimilation period. Differing degrees of improvement from the assimilation methods depend on the weather pattern, with the MU method generally performing better in the simulation of isolated thunderstorms and other weakly forced deep convection. Biases in the precipitation, moisture, and temperature fields of the simulations also are examined and sometimes differ considerably between assimilation schemes. Based on performance and bias, the newly developed MU method is shown to be a viable alternative to the FO method, exhibiting utility in producing and locating thunderstorms where observed and providing a better analysis at low computational cost.

CHAPTER ONE

INTRODUCTION

Many destructive weather phenomena, including extratropical and tropical cyclones, severe thunderstorms, and flash flood producing storms contain lightning. Lightning data provide an opportunity to locate areas where deep convection associated with these phenomena is occurring (e.g., Schultz et al. 2011, Rudlosky and Fuelberg 2013). By assimilating observed lightning data into numerical weather prediction models, there is hope that forecasts can be improved since convection often is poorly forecast. With the scheduled launch of the GOES-R satellite and its Geostationary Lightning Mapper (GLM) instrument in 2015 (Goodman et al. 2013), continuous lightning observations will be available over the continental United States and traditionally data-sparse regions of the Western Hemisphere. Consequently, a lightning data assimilation method has appreciable potential to advance weather prediction.

Several procedures have been developed for assimilating observational data into numerical models, including three-dimensional variational analysis (3DVAR; e.g., Hu et al. 2006, Xiao and Sun 2007), four-dimensional variational analysis (4DVAR; e.g., Mahfouf et al. 2005, Lopez 2011), ensemble Kalman filter (EnKF; e.g., Tong and Xue 2005, Dowell et al. 2011), and four-dimensional data assimilation (FDDA) nudging (e.g., Krishnamurti et al. 1991, Manobianco et al. 1994). Each of these methods utilizes an observation operator to translate model prognostic variables or control variables on the model grid to quantities represented by the observational data, or vice-versa in the case of nudging. The observation operator for some parameters may be nonlinear, which often prevents the variational and EnKF methods from finding an optimal analysis from the available data (Marecal and Mahfouf 2003).

A simple, yet accurate observation operator does not exist for lightning since lightning most directly represents electrical fields that typically are not a model prognostic variable. Translating traditional model prognostic variables such as temperature or wind, or even less traditional model prognostic or control variables such as graupel or vertical velocity, into an electric field requires a complex and nonlinear set of equations that still may not represent flash occurrence to a sufficient degree of accuracy (e.g., Mansell et al. 2005, Kuhlman et al. 2006, Barthe and Pinty 2007, Fierro et al. 2008). Furthermore, adequately relating hydrometeors to thermodynamic parameters requires considering the time evolution of the model to assure

dynamical consistency, which makes successful applications into 3DVAR difficult. Although 4DVAR and EnKF can consider the time evolution of a simulated storm when assimilating lightning data, the nonlinear moist physics that represent thunderstorms are difficult to properly linearize and to construct an adjoint model for 4DVAR. Integrating the model backwards with an inadequate adjoint model will yield a suboptimal analysis (Park and Zupanski 2003, Errico et al. 2007). The nonlinear nature of a potential lightning observation operator, as well as the processes that generally represent thunderstorms, along with other issues, have been obstacles to assimilating lightning data with the sophisticated variational or EnKF method. Additionally, the computational cost of such sophisticated methods applied at the horizontal scales necessary to resolve thunderstorms is burdensome and impractical in an operational setting.

As a result of these myriad difficulties, especially the nonlinearities associated with representing lightning, nudging is a viable alternative to the more sophisticated variational and ensemble Kalman filter methods. Although lightning observations have been shown to be capable of modulating convection in a cloud-resolving (i.e., 4 km or less; Weisman et al. 1997) application of the EnKF when using graupel volume as a proxy for lightning flash rates (Mansell 2013, Allen and Mansell 2013), nudging methods mostly have been used for assimilating lightning data due to their simple, computationally inexpensive way of producing convection while maintaining a dynamically consistent model solution.

Since electrical information is not typically a model prognostic variable, a proxy for lightning must be used in assimilation. Many previous approaches have used latent heating and/or increasing the relative humidity as a proxy for observed lightning. These proxy choices are well suited for coarse resolution and parameterized convection, which characterized most of these nudging applications. One of the first tests of this type of lightning assimilation was the simulation of an extratropical cyclone (Alexander et al. 1999). Their effort was based on the work of Manobianco et al. (1994) and Jones and Macpherson (1997) who had used precipitation rates derived exclusively from polar-orbiting microwave and geostationary infrared imagery to either increase or decrease latent heating rates, and hence modulate convection through nudging. They also increased relative humidity at levels where the latent heating rate had been increased as part of the assimilation. Alexander et al. (1999) found that including lightning data to derive the rain rates used in modifying the latent heating rates greatly improved the quality of simulated precipitation and pressure fields. This lightning data assimilation method was further verified by

Chang et al. (2001) using an alternative rainfall-flash rate relationship. Chang et al. (2001) concluded that accurately locating the lightning and precipitation was more important than accurately determining the intensity of the convection.

The latent heating nudging method of assimilating lightning data also has been applied using data solely from the Pacific Lightning Detection Network (PacNet; Pessi and Businger 2009b). The precipitation rates were derived from an a priori rainfall-flash rate relationship using PacNet lightning data and rain rates from the precipitation radar on the Tropical Rainfall Measuring Mission (TRMM) satellite (Pessi and Businger 2009a). Since only lightning data were used to infer the observed rain rates and latent heating rates, the simulated latent heating rates were not set to zero in locations where the model produced deep convective rainfall, but no lightning was observed.

A related latent heating based diabatic digital filter initialization (DDFI) assimilation method currently is part of the Rapid Refresh (RAP) assimilation procedure (Weygandt et al. 2008). The DDFI first performs a backward adiabatic integration, then assimilates latent heating rates derived from both radar reflectivity and lightning data, and lastly integrates the full diabatic model forward to the analysis time. The process allows both enhancement and suppression of convection and modifies the wind field to assure the assimilated latent heating rates are better retained.

Lightning data assimilation methods developed by Papadopoulos et al. (2005) and Mansell et al. (2007) only increased humidity instead of also increasing latent heating rates to enhance convection. These methods were based on techniques to assimilate radar reflectivity data by Gallus and Segal (2001) and Rogers et al. (2000). The Gallus and Segal (2001) assimilation scheme increased relative humidity to 80% at levels below -10°C in locations where organized radar echoes were observed at the model initialization time. Using this method, Gallus and Segal found appreciable improvement in precipitation forecasts utilizing both the Kain-Fritsch (KF; Kain and Fritsch 1993) and Betts-Miller-Janjic (BMJ; Betts 1986, Betts and Miller 1986, Janjic 1994) cumulus parameterization schemes (CPS). In contrast to improvements from assimilating radar data, Gallus and Segal (2001) found little to no improvement when assimilating mesoscale surface observations or using a cold pool initialization scheme. Papadopoulos et al. (2005) also increased humidity by nudging a model utilizing the BMJ CPS. They nudged their model toward empirically-derived specific humidity profiles at locations

where lightning was observed, regardless of whether the model had produced convection. The method nudged all levels of the troposphere and only allowed humidity to increase. Although the intensity of the nudging was a function of the observed flash rate, no suppression of convection was undertaken where the model produced deep convection but no lightning was observed. Radar reflectivity data also were used by Rogers et al. (2000) to control the KF CPS and increase the humidity where needed. Where observed reflectivity values exceeded 40 dBz but deep convection was not apparent in the model, moisture was incrementally added to the parcel source layer until a 4 km cloud depth was present or the added moisture equaled 1.0 g kg^{-1}. Where the CPS indicated deep convection but observed reflectivity values were not sufficiently large, all convective tendencies were set to zero. A lightning data assimilation method closely resembling that of Rogers et al. (2000) was developed by Mansell et al. (2007). Like Rogers et al. (2000), Mansell et al. (2007) utilized the KF CPS to control convection, but instead of radar reflectivity denoting deep convection, lightning flash rates exceeding a certain threshold were used to denote the areas of deep convection. The above studies all illustrate how relative humidity can be increased to initialize deep convection and indirectly force more accurate profiles of heating rate. In contrast, the current research investigates whether the low levels of the vertical temperature profile can be modified to achieve the same results.

A nudging method utilizing relative humidity to assimilate lightning data appropriate for cloud-resolving scales was developed by Fierro et al. (2012). They used total lightning data from the Earth Networks Total Lightning Network (ENTLN) mapped on a 9 km grid to mimic that of the proposed GLM. At locations where lightning was observed, the relative humidity was increased in the mixed phase region (0 to -20°C) according to a hyperbolic tangent function of flash rate and simulated graupel mixing ratio. The humidity was increased to a possible range of 81%-101% only when the existing relative humidity was less than 81%. Subjective verification found that simulations using their lightning data assimilation method produced precipitating convection that was better colocated with observed reflectivity fields than simulations not using their assimilation method. A potential shortcoming of moistening to produce deep convection is that large amounts of water vapor may need to be added to the model which would produce a moist bias in the humidity field.

This study develops and tests an alternative method of assimilating lightning data that is intended for cloud-resolving scales. Our method promotes convection by warming a layer

instead of moistening it at those locations where lightning is observed. Unlike previous methods that effectively warmed the mid and upper-troposphere by increasing latent heating, the current warming is prescribed in the updraft source layer. This procedure of warming to initiate or strengthen updrafts that produce a storm is conceptually similar to methods that primarily increased humidity. Previous moistening methods sought to have the full-physics model itself determine the convective heating profiles appropriate for a storm and its environment, in contrast to arbitrarily inserting or augmenting the latent heating profiles directly. The objective of our new method is to modify the model field just enough to produce storms in the correct location. The approach is based on the assumption that the model thermodynamic profiles are reasonably accurate and that the model merely needs a slight modification to initiate deep convection. Warming in the lower troposphere is hypothesized to be a way to maintain a better conservation of moisture and to achieve the objective of minimal modification while also producing a better analysis and resulting forecast.

CHAPTER TWO

METHODOLOGY

2.1 Model Configuration and Case Studies

The three-dimensional, fully compressible, non-hydrostatic Weather Research and Forecasting Model (WRF) with the Advanced Research dynamic solver (WRF-ARW, Version 3.4.1; Shamarock and Klemp 2007) was used in this study. All simulations utilized two-way nesting between three domains: an outer domain of 27 km horizontal grid spacing, an intermediate domain of 9 km grid spacing, and an inner domain of 3 km grid spacing, all with 60 vertical levels. Assimilation was implemented on the 9 and 3 km domains; no assimilation was performed on the outermost 27 km domain. Results presented in chapter 3 focus on the 3 km domain. Simulations utilized the WRF single-moment 6-class bulk microphysics scheme (WSM6; Hong and Lim 2006), the Mellor-Yamada-Janjic turbulence kinetic energy planetary boundary layer scheme (MYJ-TKE; Janjic 1994), the Noah land surface model (Chen and Dudhia 2001, Ek et al. 2003), Dudhia (1989) shortwave, and Rapid Radiative Transfer Model longwave radiation scheme (RRTM; Mlawer et al. 1997, Iacono et al. 2000). The Kain-Fritsch CPS (Kain and Fritsch 1993) was utilized on the outermost domain, while no CPS was utilized on either the 9 or 3 km domains. This is similar to Hu et al. (2006) who did not use CPS on a 9 km model grid because they found worse results from the nested 3 km domain when utilizing the KF CPS on the 9 km domain with no CPS on the 3 km domain. Hu et al. (2006) also similarly assimilated cloud information utilizing a 3DVAR method for a tornadic case in the South Central United States.

We ran simulations for three severe thunderstorm cases over the United States. The cases include the extensive outbreak of deadly supercell tornadoes on 27 April 2011 and a squall line causing numerous severe wind reports across the Southeast on 15 June 2011. The third case involved a mixture of organized squall line features over the Northeast and Midwest and more isolated deep convection across the southern Appalachians on 9 June 2011 causing numerous severe hail and wind reports. All three of these days were among the most electrically active for the Eastern United States during 2011.

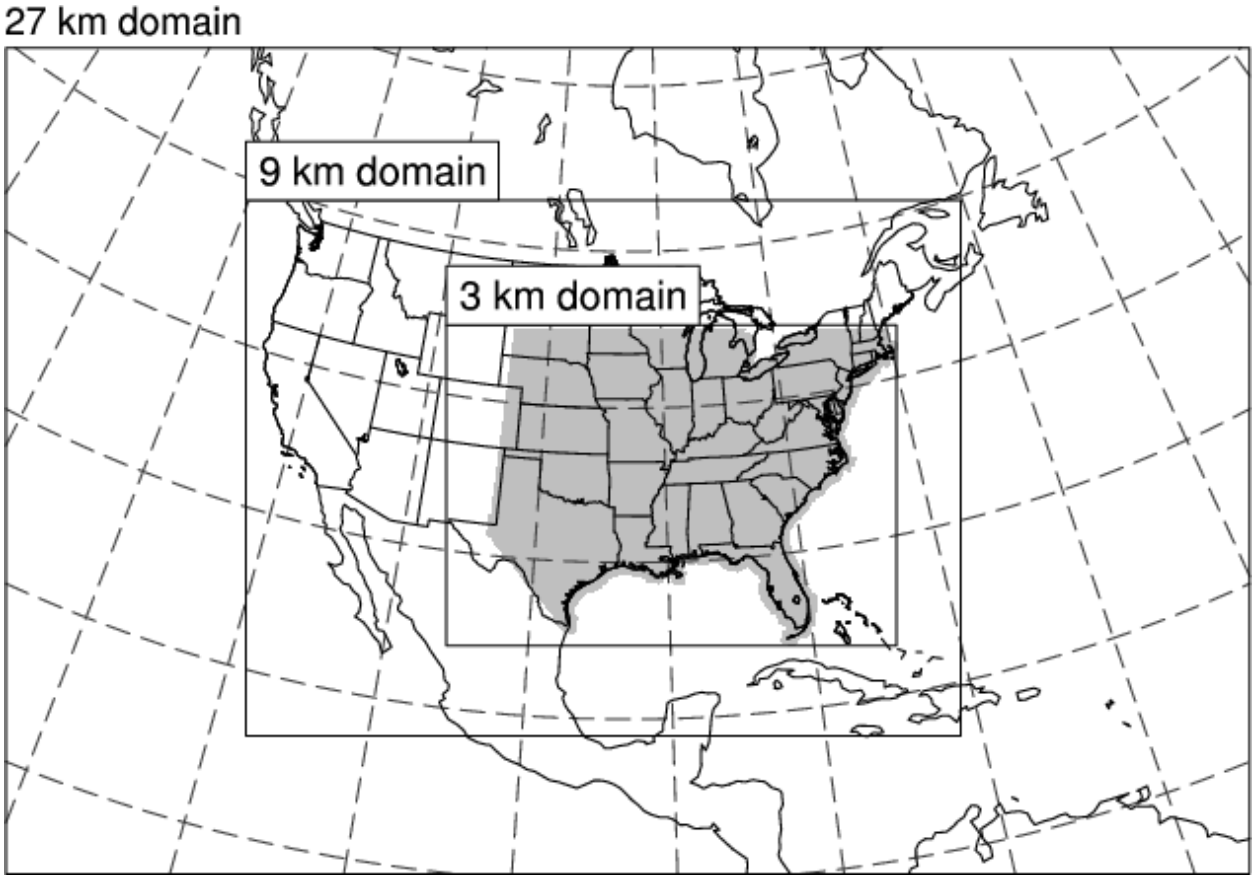

Fig. 1. Domains of the 27, 9, and 3 km horizontal grid spaced regions along with the precipitation verification domain (shaded grey) used in chapter 3.

The outer 27 km domain for all three cases included the Caribbean Sea and large portions of the Atlantic and Pacific Oceans (Fig. 1). The areal extent of the 9 km domain contained the entire contiguous United States, while the 3 km domain covered the U.S. east of the Rocky Mountains. All of the severe storm simulations included 6 h of model spin-up between 0600 UTC and 1200 UTC, after which lightning assimilation began and continued for 12 h. The simulations then were run an additional 12 h without assimilation, ending on 1200 UTC of the next day. The spin-up period allows more realistic small-scale features in the model fields to be present in the simulation. These small-scale features are not present at the start of the spin-up period in the 3 km domain simulations since model fields are interpolated from the 1˚ NCEP Final Operational Global Analysis (FNL). By assimilating after the spin-up period, assimilation is more like that of a continuous data assimilation system commonly employed operationally (Kasahara et al. 1988). The model simulations employed in Mansell et al. (2007) and Fierro et al.

(2012) also allowed model spin-up before assimilating lightning data. We performed tests without using the spin-up period, but assimilation results were similar and are not shown.

Six-hourly 1˚ NCEP Final Operational Global Analysis (FNL) data were used as initial and lateral boundary conditions for all three cases. Although simulations also were tested with 6-hourly 40 km North American Mesoscale Model (NAM) analyses, those employing FNL data generally produced better precipitation forecasts, both when assimilation was used and when it was not (not shown).

2.2 Lightning Data

We assimilated lightning observations from the Earth Networks Total Lightning Network (ENTLN; http://earthnetworks.com/Products/Total LightningNetwork.aspx). The ENTLN has sensors worldwide that detect total lightning: both intra-cloud (IC) and cloud-to-ground (CG). In the area of the 3 km model domain, the location accuracy for the ENTLN is less than 400 m, with the CG detection efficiency exceeding 95% over land. IC detection efficiency is less, generally in the 50-90% range (see Fig. 6 of Fierro et al. (2012)). Each total lightning flash was specified by a latitude, longitude, and time to a fraction of a second.

Before each model integration time-step, the lightning flashes were binned and summed onto the intermediate 9 km domain grid using the location and time information. If a flash was located within a model grid cell and occurred ± 5 min from the current simulation time, a flash was added to the count of that grid cell. For example, if the model was initialized at 1200 UTC with a time step of 30 s and a flash occurred in a grid cell 1 s before 1200 UTC, then the flash contributed to the flash count of the grid cell at the model initialization time. After 10 model time-steps the simulation time would be 1205 UTC, and since the flash occurred before the 1200 UTC limit of the 10 min window, that flash would not contribute to the flash count of the cell. Thus, the flash count at each model grid cell is effectively a flash rate density of integer values with units of flashes $(10\ \text{min})^{-1}$ $(9\ \text{km})^{-2}$. Using those units allowed each of the nine 3 km grid cells contained in the intermediate 9 km domain to be assigned the same flash rate density as the encompassing 9×9 km grid cell. The flash rate densities from the 9 km domain grid were used when assimilating on the innermost 3 km domain so the grid spacing of the assimilated lightning data would approximate that of the upcoming GLM. Our assimilation method does not depend

on the intensity of the lightning flash rate density but only considered whether no flashes or one or more flashes occurred in each grid cell.

2.3 Warming to Initiate Deep Convection

Our assimilation procedure is based on parcel theory despite its several well known limitations (e.g., Markowski and Richardson 2010). A parcel that is warmer than its environment is buoyant and more likely to reach its level of free convection (LFC) and form a cloud. If the equilibrium level (EL) associated with this parcel is high enough and entrainment is not overly debilitating, a storm can develop. If the parcel is not warm enough to reach its LFC, or if the EL is too low to produce deep convection, the parcel can be warmed in an effort to eradicate convective inhibition (CIN) below the LFC, raise the EL, and thereby increase the parcel's convective available potential energy (CAPE). Even in a low humidity environment, enough warming in the source layer will eventually cause a thunderstorm to form.

Warming near the surface to initiate convection at a desired location is not a new concept in cloud modeling. Idealized and cloud-scale simulations of convection, including supercells, frequently use a thermal perturbation or warm bubble to initialize convection (e.g., Weisman and Trapp 2003, Lericos et al. 2007, Barthe et al. 2010). The warm bubble is an ellipsoid of positive potential temperature perturbation near the surface and typically located near the center of the domain. The potential temperature perturbation decreases with radial distance from the ellipsoid's center until reaching zero at a specified distance (Klemp and Wilhelmson 1978). The warm bubble approach generally is used in favor of other initiation methods such as modifying the model wind field (Loftus et al. 2008) or directly inserting an updraft (Naylor and Gilmore 2012).

Inserting a warm bubble can cause superadiabatic layers and may induce excessive modification of the simulation. Therefore, our nudging method warms the model profile to the convective temperature determined from the convective condensation level (CCL). This consequently allows us to consider the near surface temperature and humidity profiles of a grid column when determining the temperature profile to nudge toward. This method potentially prevents more warming than necessary to create deep convection. This is achieved since warming dry adiabatically down from the CCL typically will produce a cloud and allow the cloud to access CAPE without the need for mechanical lifting.

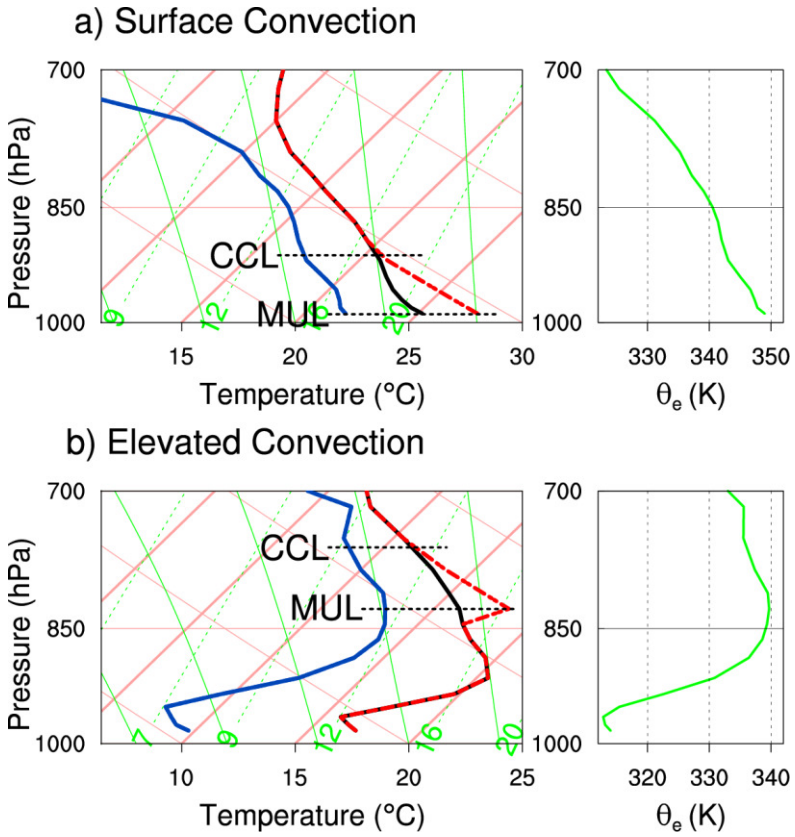

Fig. 2. Temperature profile (red dashed line) obtained from the MU method. Simulated temperatures are nudged toward this profile for a case with the most unstable level at the surface (a) and elevated (b). Also displayed are the preexisting temperature (black solid line) and the unmodified dew point temperature profile (blue solid line). On the right side are the preexisting equivalent potential temperature profiles (θ_e; green solid line) used to calculate the most unstable layer for the respective cases.

A convective temperature that is calculated from a surface-based CCL is not appropriate for all environments since both surface-based and elevated convection occur in the atmosphere. To account for the possibility of elevated convection, the CCL and associated convective temperature were calculated from the most unstable level (MUL) of each grid cell's sounding. The MUL is the altitude of maximum equivalent potential temperature and represents the level from which the most buoyant parcels will initiate. The MUL is commonly used in convective parameterizations such as the BMJ (Baldwin et al. 2002) and to calculate the most unstable CAPE (e.g., McCaul and Cohen 2002, Rudlosky and Fuelberg 2011). Figure 2 illustrates temperature profiles that the assimilation procedure would nudge toward for two hypothetical situations: when lightning is occurring where the MUL is the surface (Fig. 2a), and where the

MUL is elevated just above 850 hPa (Fig. 2b). Only model levels up to 700 hPa were considered in finding the maximum equivalent potential temperature and associated MUL.

A second method to initialize deep convection was also tested, but produced unsatisfactory results. This method cooled the environmental temperature profile to the parcel temperature between the lifting condensation level and LFC. The cooling however produced negatively buoyant air that tended to cause descent. This descending motion then deterred deep convection from forming.

2.4 Newtonian Nudging

Newtonian relaxation, or nudging, (Anthes 1974) is a form of FDDA commonly used to modify the model mass and/or wind field during integration based on observed temperature, wind, and humidity. The procedure seeks to nudge the model toward these observations while limiting the introduction of possible dynamical imbalances that could cause an unstable solution. By slowly nudging toward observations, geostrophic adjustment is allowed to occur in response to the atmospheric information supplied by the observations. How strongly forced the nudging occurs depends on a nudging coefficient (G) of the general form:

$$d\alpha/dt = F + G \times (\alpha_o - \alpha), \quad (1)$$

where α is a prognostic variable, α_o is the observation associated with that variable, and F is the forcing term for that variable supplied by the model.

The previously cited lightning assimilation methods did not use traditional Newtonian nudging. Instead, the methods modifying latent heating merely increased existing model heating rates included in the F term of (1) by a factor dependent on the derived rain rate. Therefore, model imbalances would be small when increasing F, despite modifying a large component of the mass field. Since the added humidity has only a small effect on the mass field, model stability is not a major consideration. In the method developed by Fierro et al. (2012), the desired humidity value was directly inserted without any apparent stability issues. Newtonian nudging also typically entails defining a radius of influence, i.e., the distance from the observation that information is spread onto the analysis. Pessi and Businger (2009b) defined a specific radius of influence. The radius of influence for the other cited methods can be interpreted as being proportional to the grid spacing of the lightning data being utilized.

The typical value of the nudging coefficient (G) in (1) has been on the order of 10^{-4} s^{-1}, representing an e-folding time of 1-3 h (Stauffer and Seaman 1990). Since nudging traditionally has been performed on the synoptic and meso-alpha scales, 1-3 h represents an appropriate time-scale for those applications. However, when assimilating in areas of thunderstorms which may have a life cycle less than 1 h, this value is too small. We tested nudging coefficients of 5×10^{-3} s^{-1}, 0.01 s^{-1}, 0.02 s^{-1}, and 0.04 s^{-1}, with 0.01 s^{-1} generally performing best (not shown). Results showed that at values exceeding ~ 0.04 s^{-1}, temperature on the intermediate 9 km domain is nudged to the intended profile in only one or two time steps. This rapidity can create an unstable model solution. Although the chosen nudging coefficient is too large to allow for geostrophic adjustment, it does allow for hydrostatic adjustment to occur through buoyancy and acoustic waves (Chagnon and Bannon 2005). If the nudging coefficient represents a relaxation time near that of the model time step, then the model solution is overrun with high frequency acoustic waves resulting in an unstable model solution. Since thunderstorms occur at small spatial as well as temporal scales, we did not employ a radius of influence; instead assimilation only was performed if at least one lightning flash occurred on the intermediate 9 km grid described in section 2.2.

We did test to see if defining G to be dependent on the flash rate density would produce better results. In the test, if more lightning was observed, then G would be increased to more rapidly warm areas of intense lightning relative to a grid cell that may have only one flash observed. This had an insignificant impact on the simulation and unnecessarily complicated the assimilation method. Consequently, there is no dependency on the lightning flash rate in our method employed during the simulations shown later.

2.5 Denoting Deep Convection Using Maximum Graupel Mixing Ratio

If observations indicate lightning in a model grid cell, that cell must be checked for the presence of simulated convection that is sufficiently intense to hypothetically produce the lightning. If the simulation suggests lightning activity at a grid cell where it is observed in nature, additional convection should not be induced. Thus, it is important to define a metric that is easily computed from the model variables and well correlated with lightning flash rate.

Non-inductive charging is widely believed to be the primary mechanism causing thunderstorm electrification (e.g., Vonnegut 1963, Takahashi 1978, Saunders 1993). Non-

inductive charging results from collisions between graupel, ice crystals, and supercooled water. For this to occur, vertical velocities must be sufficiently strong at temperatures less than 0˚C. This explains the high correlation between lightning and updraft velocity (Price and Rind 1992, Pickering et al. 1998). If updrafts are sufficiently strong, graupel can be produced. As a result, graupel mass flux at -15˚C and vertically integrated ice mass are two metrics that have been associated with lightning flash rate (McCaul et al. 2009). Unfortunately, vertical velocity and vertically integrated ice mass depend on model resolution as well as the microphysics parameterization scheme being used. Use of graupel mass flux compounds the resolution sensitivity issue since it is a product of both vertical velocity and graupel mass. Vertically integrated ice mass likely is less sensitive to model grid spacing, but large values can occur in stratiform winter precipitation areas not containing lightning. Although a metric such as cloud depth above freezing level (Futyan and Del Genio 2007) may be less sensitive and useable with parameterized convection, it can be difficult to define a cloud and the computations may be burdensome.

Due to graupel's association with lightning and its ease of computation, we selected maximum graupel mixing ratio in a grid column (qgmax) as the model derived metric to denote deep convection that is sufficiently intense to produce lightning. The metric was used to determine where and when our data assimilation method would be deployed. If qgmax exceeded a certain threshold and lightning was observed, no assimilation was performed. Several thresholds of qgmax were tested: 0.5 g kg^{-1}, 1.0 g kg^{-1}, 2.0 g kg^{-1}, 4.0 g kg^{-1}, 8.0 g kg^{-1}, and ∞ (i.e., no threshold). Similar to the behavior of the nudging coefficient, larger values of the qgmax threshold produced larger areas of assimilation and warming that forced deep convection. Tests revealed less sensitivity to the qgmax threshold than to G. A qgmax threshold of 1.0 g kg^{-1} generally produced the best results (not shown) and was used for all simulations. This qgmax value is suitable since most simulated storms with maximum updrafts of 10 m s^{-1} or more extending above the freezing level will have graupel mixing ratios exceeding this value.

2.6 Verification with NCEP Stage IV Precipitation Observations

The simulated precipitation fields were verified against hourly precipitation from the gridded NCEP stage IV dataset. Stage IV data are determined from radar and rain gauge observations and benefit from human quality control at the National Weather Service River

Forecast Centers (Lin and Mitchell 2005). The observations cover much of the contiguous United States. The 3 km simulated precipitation data were interpolated to the approximately 4 km stage IV grid. However, verification of precipitation only included the data points in the verification domain (grey shading in Fig. 1). The verification domain ensured the use of only high quality stage IV data over or near land in the United States east of the Rocky Mountains.

Our verifications utilized equitable threat score (ETS; Schaefer 1990), frequency bias (BIA), and probability of false detection (POFD). These were calculated based on a 2×2 contingency table of forecast and observed binary hourly precipitation events exceeding a certain threshold (Wilks 1995). Three hourly precipitation thresholds were used: 1 mm, 5 mm, and 10 mm. The contingency table consists of hits (a), false alarms (b), misses (c), and correct null events (d) to calculate the metrics:

$$\mathrm{ETS} = \frac{a - a_{ref}}{a + b + c - a_{ref}}, \tag{2}$$

$$a_{ref} = \frac{(a + b)(a + c)}{a + b + c + d}, \tag{3}$$

$$\mathrm{BIA} = \frac{a + b}{a + c}, \quad \text{and} \tag{4}$$

$$\mathrm{POFD} = \frac{b}{b + d}. \tag{5}$$

An ETS of 1.0 represents a perfect score, but values can be as small as -1/3, with negative values indicating a forecast whose skill is worse than a random forecast. Although ETS can over reward a biased forecast (Hamill 1999), it still is useful because it rewards high-bias forecasts less than the threat score (TS) or critical success index (Gandin and Murphy 1992; Baldwin and Kain 2006). ETS differs from TS by including the a_{ref} term (3) which represents the number of hits realized by chance.

Frequency bias, or bias score, (BIA; 4) ranges from 0 to infinity, with values less than 1 indicating underforecasting of precipitation amounts of a specified threshold relative to the stage IV observations, whereas values greater than 1 indicate overforecasting. POFD (5) represents the fraction of false alarm forecasts relative to the number of precipitation forecasts not exceeding a specified threshold.

A neighborhood spatial verification method, the fractions skill score (FSS; Roberts and Lean 2008), also was used. FSS penalizes small displacement errors of precipitation features less than ETS. This characteristic is particularly valuable when verifying simulations with small horizontal grid spacing. FSS is a variation of the fractions Brier score (FBS; Roberts 2005)

which provides leniency by defining a neighborhood region that is centered on a grid cell of the verification domain and encompasses surrounding grid cells. The simulated (P_M) and observed (P_O) fractions of grid cells located in the defined neighborhood and characterized by precipitation amounts greater than a specified threshold are used to calculate FBS:

$$\mathrm{FBS} = \frac{1}{N} \sum_{i=1}^{N} \left(P_M(i) - P_O(i)\right)^2, \tag{6}$$

where N is the number of total valid grid cells in the verification domain. FBS ranges from 0 to 1, with 0 representing a perfect simulation. A deceptively small FBS can occur when the simulated and observed areas of rain exceeding the threshold are small, regardless of whether the grid cells with observed or simulated fractions greater than zero agree well with each other. FSS provides a better comparison between different simulations or thresholds by dividing the FBS by a hypothetical worst case FBS (FBS_{worst}) from the given simulated and observed fractions:

$$\mathrm{FSS} = 1 - \frac{\mathrm{FBS}}{\mathrm{FBS}_{worst}}, \tag{7}$$

where

$$\mathrm{FBS}_{worst} = \frac{1}{N} \left(\sum_{i=1}^{N} \left(P_M(i)\right)^2 + \sum_{i=1}^{N} \left(P_O(i)\right)^2 \right). \tag{8}$$

FSS defined in this way ranges from 0 to 1, with 1 representing a perfect simulation. If BIA is 1, indicating no bias, then FSS will asymptotically approach 1 as the size of the neighborhood becomes larger and encompasses the entire verification domain. Although biased forecasts generally are penalized by FSS, the more biased forecasts sometimes yield better scores for small sample sizes and small neighborhood areas (Mittermaier and Roberts 2010).

Instead of using a square neighborhood to calculate FSS, we used a circular neighborhood with a specified radius as in Schwartz et al. (2009). The same precipitation thresholds were used as when calculating ETS and the other contingency table metrics. Six different radii of influence were used: 0, 20, 40, 60, 80, and 100 km. If the center of a surrounding grid cell was farther than the radius of influence, it was not considered to be in the neighborhood.

CHAPTER THREE

RESULTS

We assessed the performance of our warming method of lightning assimilation using three simulations for each of the three severe storm cases: a control simulation (CT), a simulation using our MU method, and a simulation using the relative humidity nudging method described by Fierro et al. (2012), hereafter denoted FO. The control simulation (CT) did not employ any lightning assimilation. When implementing FO, we used the same constants they used in the hyperbolic tangent function relating relative humidity to observed total lightning flash rate density and simulated graupel mixing ratio. However, our implementation of FO differs from theirs by updating the grid of lightning flash rates at each computational time step (~ 10 s for the 3 km domain and ~ 30 s for the 9 km domain) instead of every 10 min. Fierro et al. also used a different spin-up method, a shorter 2 h assimilation window, and a finer 1 km horizontal grid spacing. The following sections present results from the innermost 3 km horizontal grid spaced domain of the simulations.

3.1 Demonstrating the Lightning Assimilation Methods

A fundamental test of lightning assimilation methods is to determine whether they induce simulated deep convection in areas where lightning is observed. We used areas of maximum graupel mixing ratio (qgmax) exceeding 1 g kg^{-1} to denote locations of simulated deep convection. These locations were compared with locations of observed lightning flash rate densities (Fig. 3). As an example, Fig. 3 shows conditions after 6 h of assimilation for the 15 June squall line case. Areas of black shading are regions where simulated deep convection overlaps with observed lightning. The top left panel showing the CT simulation (Fig. 3a) contains few areas of black shading, i.e., agreement. Conversely, the MU and FO simulations (Figs. 3b,c) produce more deep convection where lightning is observed. Comparing the MU and FO simulations, MU visually exhibits better agreement since FO has not yet produced deep convection in central Tennessee (blue arrows in Fig. 3) where a thunderstorm with a total flash rate density exceeding 100 fl $(10\ min)^{-1}$ $(9\ km)^{-2}$ is occurring. The hollow contours in Fig. 3 indicate regions of simulated deep convection where there is no corresponding observed

lightning. In central and far western Kentucky (red arrows in Fig. 3) more hollow contours and, hence, spurious simulated convection is present for the CT simulation than for MU. This reduction in spurious convection occurs even though our method does not directly suppress convection.

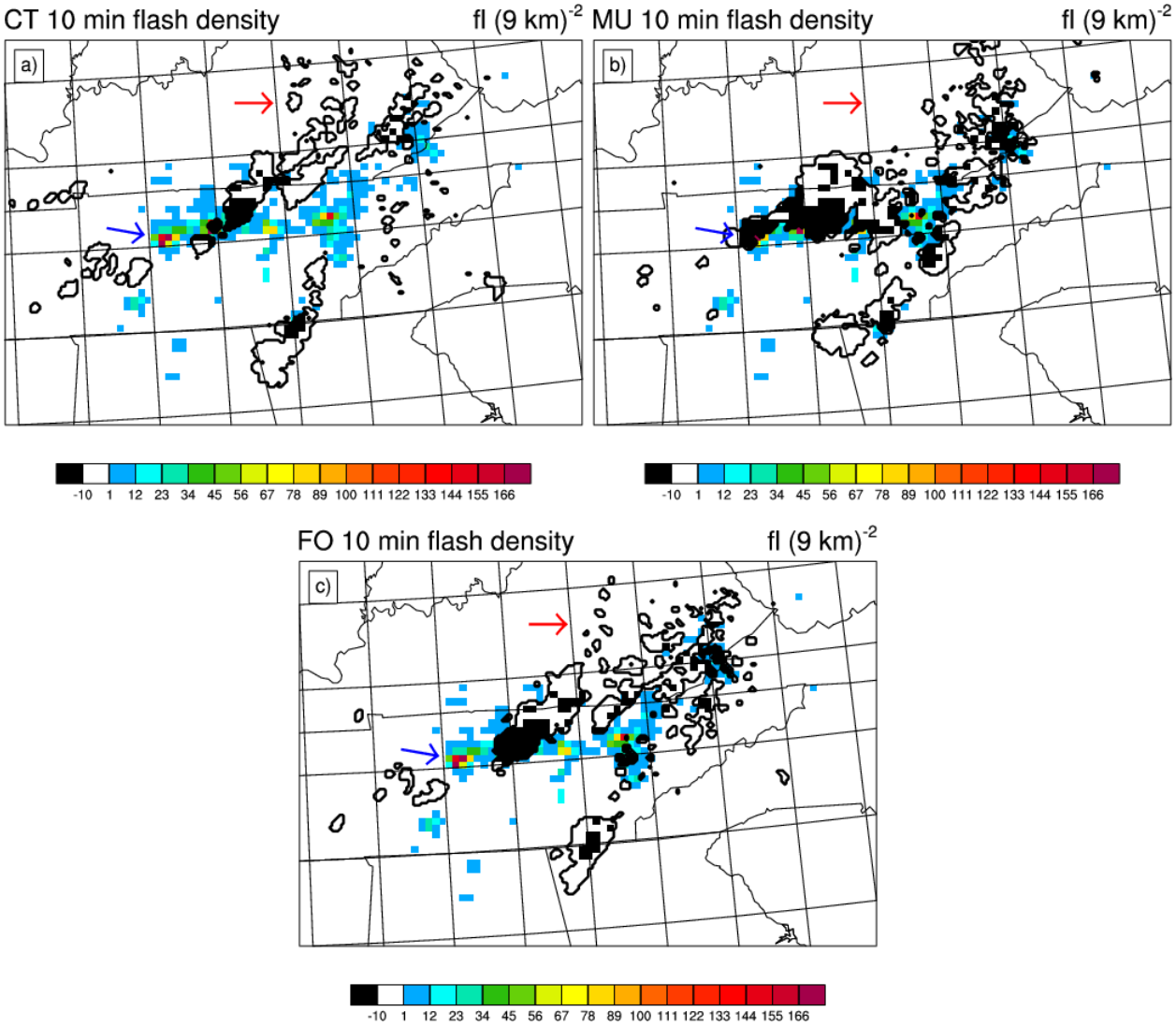

Fig. 3. Observed total lightning flash rate density over 10 min intervals (fl (9 km)$^{-2}$, shaded) with the 1 g kg^{-1} qgmax contour (in black) from the CT (a), MU (b), and FO simulations (c) at 1800 UTC 15 June 2011 (6 h after the start of assimilation). Black shading of flash rate density occurs where lightning is observed and simulated qgmax exceeds 1 g kg^{-1}, indicating agreement between deep simulated convection and observations. The hollow outlined regions denote regions of simulated deep convection where there is no corresponding observed lightning. See text for description of colored arrows.

Simulations of a persistent, nearly stationary thunderstorm occurring near the start of assimilation at 1200 UTC 9 June 2011 (location not shown) further demonstrate the effectiveness of the two assimilation methods. The stationary nature of the convection in eastern North Carolina and South Carolina allows a single grid cell to capture the time evolution of the storm. The storm also is well suited for detailed examination since it occurs at the start of the 12 h assimilation period. Thus, the effects of past modifications by MU and FO are not present. Instead, the effects of the assimilation methods are easily seen by comparing with CT.

The CT simulation fails to produce the observed storm, but does produce elevated precipitating convection 100-200 km to the southwest. The thermodynamic environment where convection is simulated by CT is similar to the environment where deep convection actually occurs (Fig. 4). Where the storm is observed, the simulated environment (black lines in Fig. 4) exhibits dew point depressions (DPD) of ~ 15-20 K in the 300-500 hPa layer. An inversion is present below 850 hPa with a DPD of 5-10 K. Where convection is erroneously simulated (not shown), the DPD is ~ 5-10 K greater between 300 and 550 hPa, which is less supportive of deep convection. At this location with erroneous convection, shallow convection is better supported with saturation near 750 hPa and mixing ratios greater by ~ 1.0 g kg^{-1} relative to the simulated environment where the storm is observed. CT does eventually produce convection, causing saturation up to ~ 500 hPa for one of the simulated storms. Since the area of observed lightning and, hence, the region of assimilation in the MU and FO simulations is ~ 100 km away, the spurious simulated convection also is present in the MU and FO simulations. The spurious convection in MU and FO exhibits only subtle differences with the CT simulated convection. The presence of this nearby convection under similar environmental conditions suggests that the simulated environment at the location of the observed storm is conducive for deep convection and sufficiently represents the observed environment. Thus, the CT sounding apparently lacks an impetus to force convection where it is observed. The MU and FO methods provide more conducive conditions and attempt to produce a storm of similar strength and characteristics of the true storm.

Five minutes into the assimilation period at the grid cell in eastern North Carolina where lightning is observed, the direct effects of the assimilation methods become apparent (Fig. 4), while the indirect effects are more subtle. Comparing soundings from the two assimilation methods with those of CT reveals the direct modifications (Figs. 4 and 5). Since there is flash

activity in this grid cell at 1200 UTC, the FO method increases the relative humidity to ~ 85% at levels between 0 and -20 ˚C (blue lines in both figures). With the most unstable level (MUL) located just above 850 hPa, the MU method dry adiabatically warms the layer extending from the CCL down to the MUL (red lines in Figs. 4 and 5). The greatest temperature difference between MU and CT is ~ 1.9 K at the MUL, which is the amount that MU directly warms the simulated sounding (red dashed line in Fig. 5).

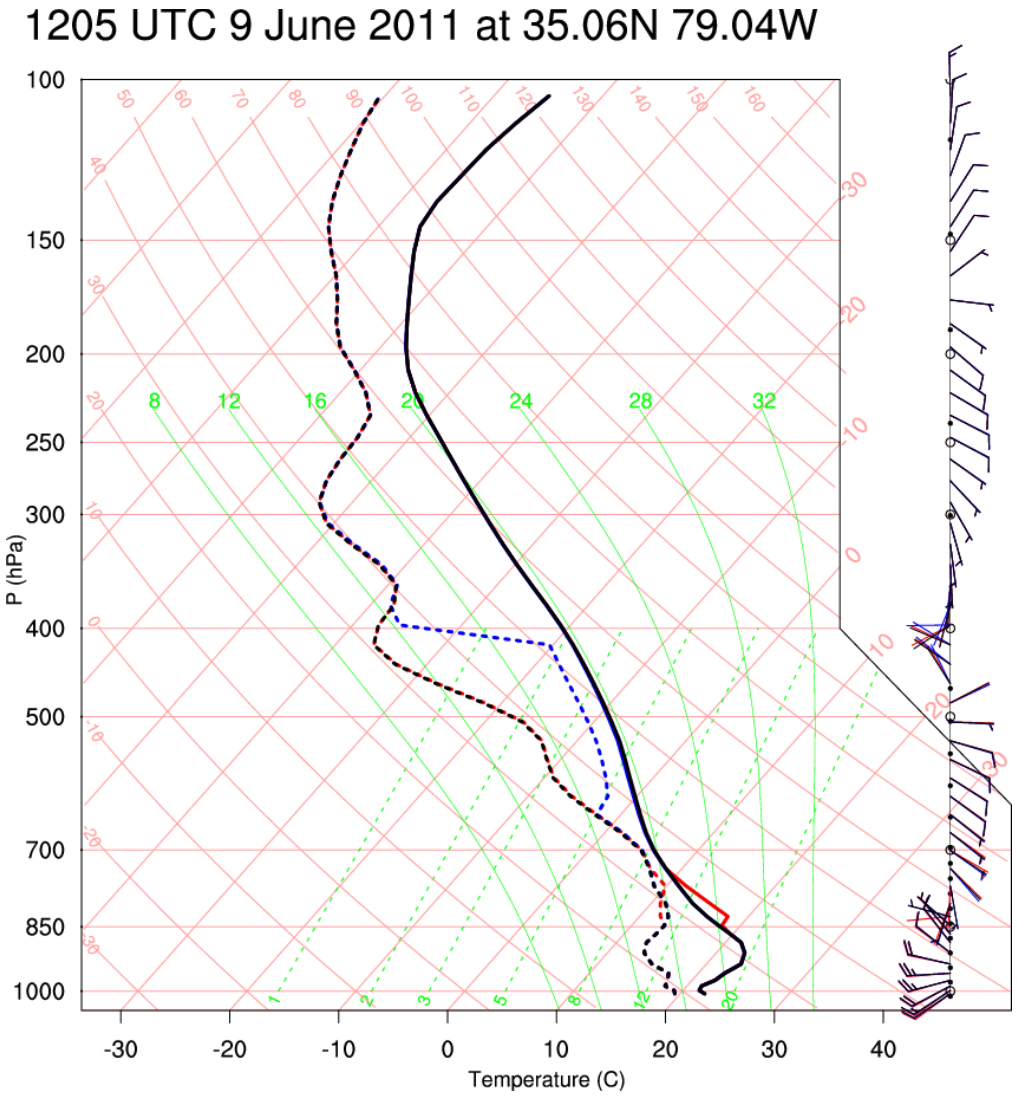

Fig. 4. Skew-T diagram at 1205 UTC 9 June 2011 (5 min after the start of lightning assimilation) at the location of observed lightning in eastern North Carolina with air temperature (°C, solid lines), dew point temperature (°C, dotted line), and horizontal wind (kt, barbs along right axis). The different colored lines represent different simulations: black for CT, red for MU, blue for FO.

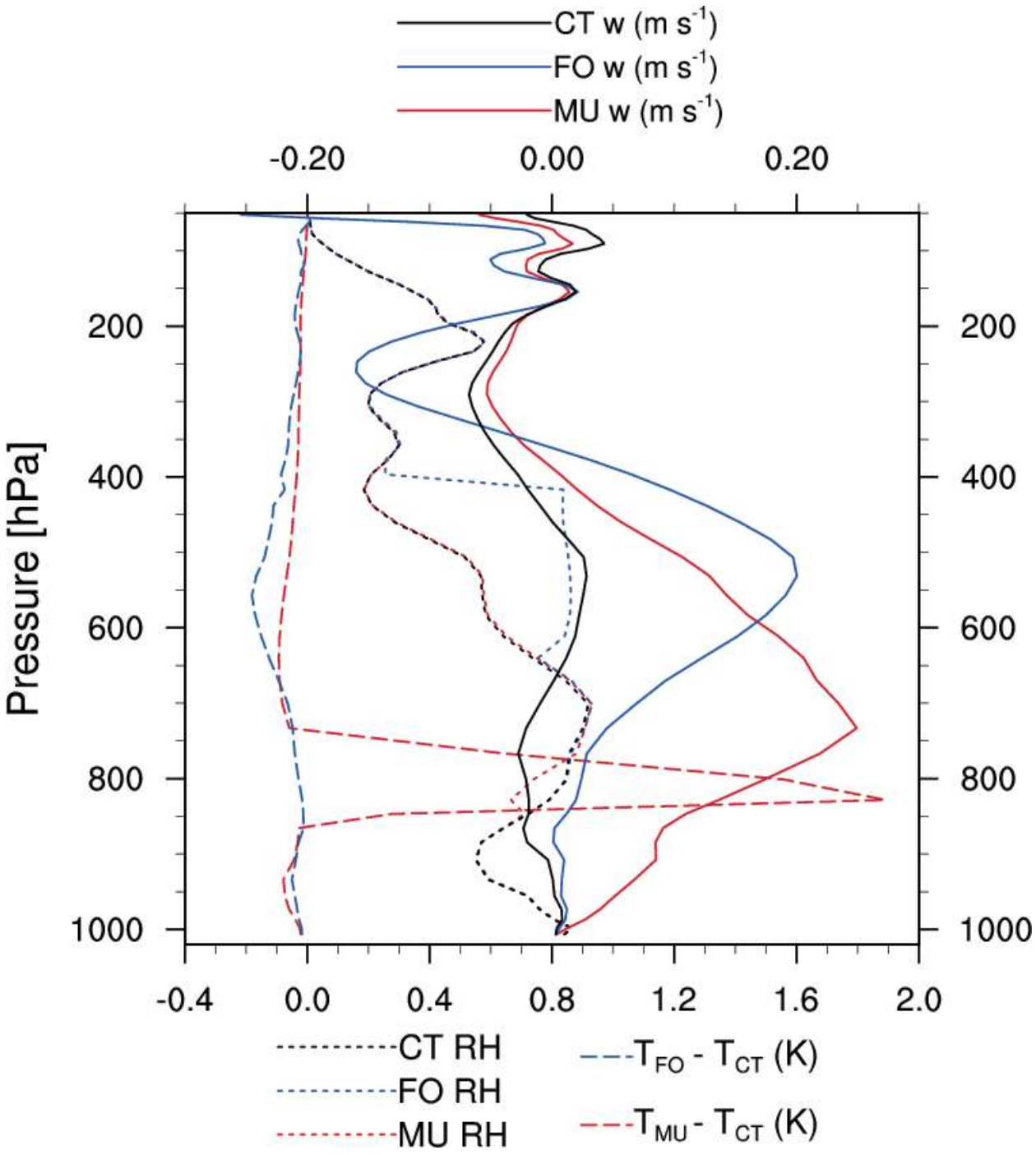

Fig. 5. Vertical profiles of vertical velocity (m s^{-1}, solid lines using top x-axis), relative humidity (a unitless fraction, dotted lines using bottom x-axis), and temperature difference between lightning assimilation method and CT simulation (K, dashed line using bottom x-axis) with the same line colors as in Fig. 4 and at the same time and location as Fig. 4, i.e., 1205 UTC 9 June 2011, 5 min after the start of lightning assimilation.

Weak indirect effects of assimilation occur as the numerical model responds to the direct modifications. Temperature and dew point profiles at 1205 UTC (5 min after assimilation begins) indicate few indirect effects of the modifications (Fig. 4). For example, when FO directly moistens a layer, the model responds by cooling the same layer only ~ 0.1 K relative to the CT simulation (dashed blue line in Fig. 5). Conversely, when using MU, dew point temperatures (dotted red line in Fig. 4) respond in the layer directly warmed. Both of these model responses are due to vertical motion resulting from the direct modifications that produce the more buoyant air (Fig. 5). Increasing the relative humidity in the layer also increases the virtual temperature (T_v) by ~ 0.3 K which causes stronger updrafts in FO than in CT (solid blue and black lines). The initiated updrafts produce cooling, which counters the warming of T_v by the FO method. Similarly, an updraft in the layer where MU produces warming (solid red lines) causes the water vapor mixing ratio (dashed red lines in Fig. 6) to become more constant with altitude. The FO simulation produces a peak updraft of ~ 0.2 m s^{-1}, while the MU simulation has a slightly stronger peak updraft of 0.25 m s^{-1}. At this early time, neither is strong compared to thunderstorms in nature that typically have updrafts exceeding 10 m s^{-1} and sometimes even 50 m s^{-1}. Also noteworthy is the FO simulation producing an updraft with an elevated peak velocity (at ~ 500 hPa) that does not extend down to the low levels compared to the MU simulation. The more elevated updraft helps explain why no substantial convection occurs at this grid cell in the FO simulation even though lightning is observed over the next few hours. Specifically, no updraft is present in the low levels to force a low-level cloud capable of accessing the available CAPE.

Although the indirect effects of assimilation are small during the first 5 min of assimilation (Figs. 4-5), the model reacts substantially after 30 min to the initial changes and subsequent smaller modifications by the MU method (Fig. 6). In the MU simulation at the same grid cell as in Figs. 4 and 5, saturation extending to ~ 500 hPa (a cloud) occurs by 1230 UTC, with the temperature lapse rate increasing to approximately moist adiabatic above ~ 700 hPa. These temperature and dew point profiles along with a peak updraft velocity of ~ 11 m s^{-1} (not shown) are indicative of a developing thunderstorm. The storm's cloud base, i.e., lowest level of saturation, is approximately the CCL that marks the top of the layer being warmed (Fig. 4). The cloud base also is at nearly the same pressure level as the nearby spurious convection produced

by the model (not shown), suggesting that the cloud base for the storm in the MU simulation is realistic.

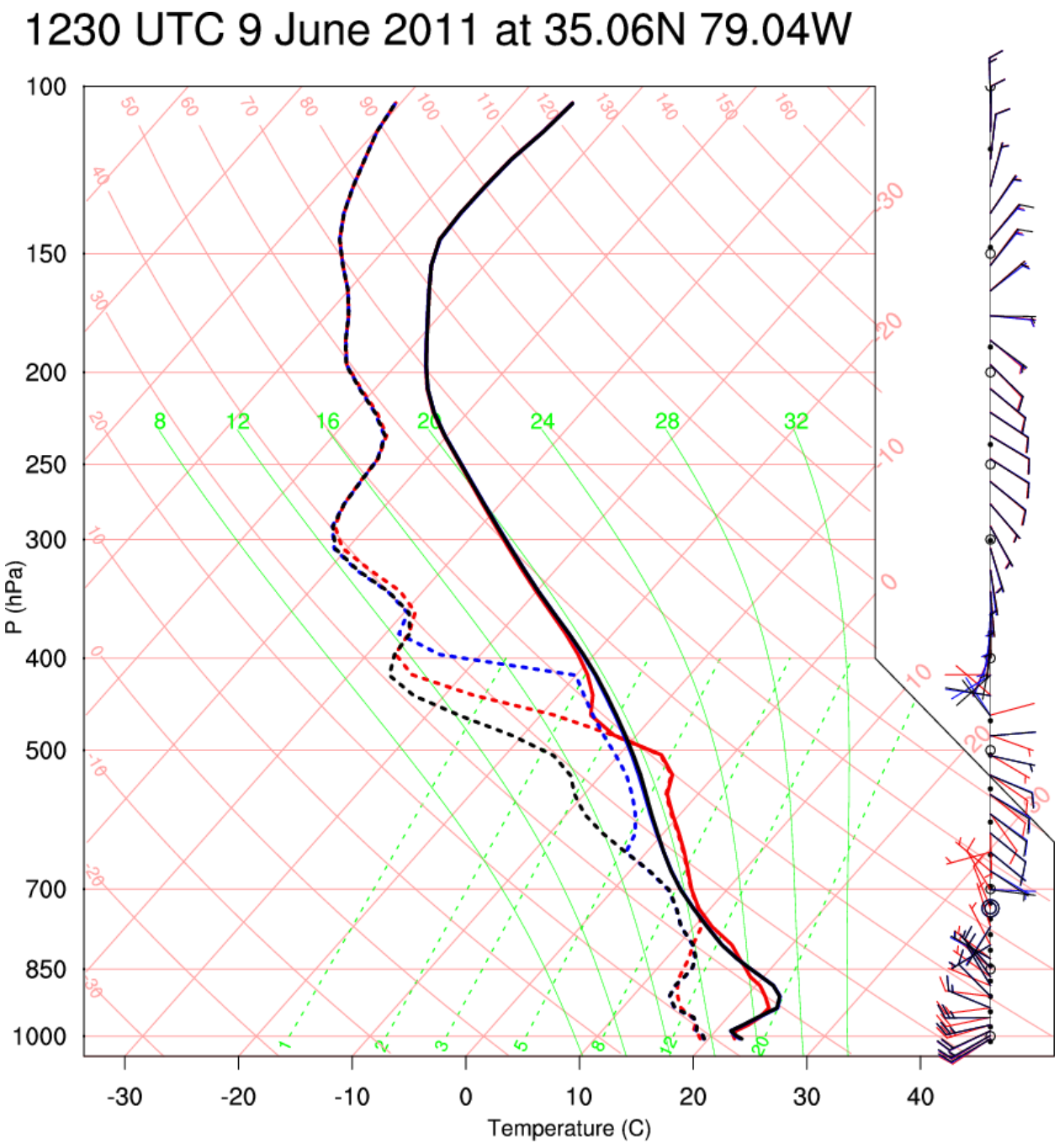

Fig. 6. As in Fig. 4, except at 1230 UTC 9 June 2011, i.e., 30 min after the start of lightning assimilation.

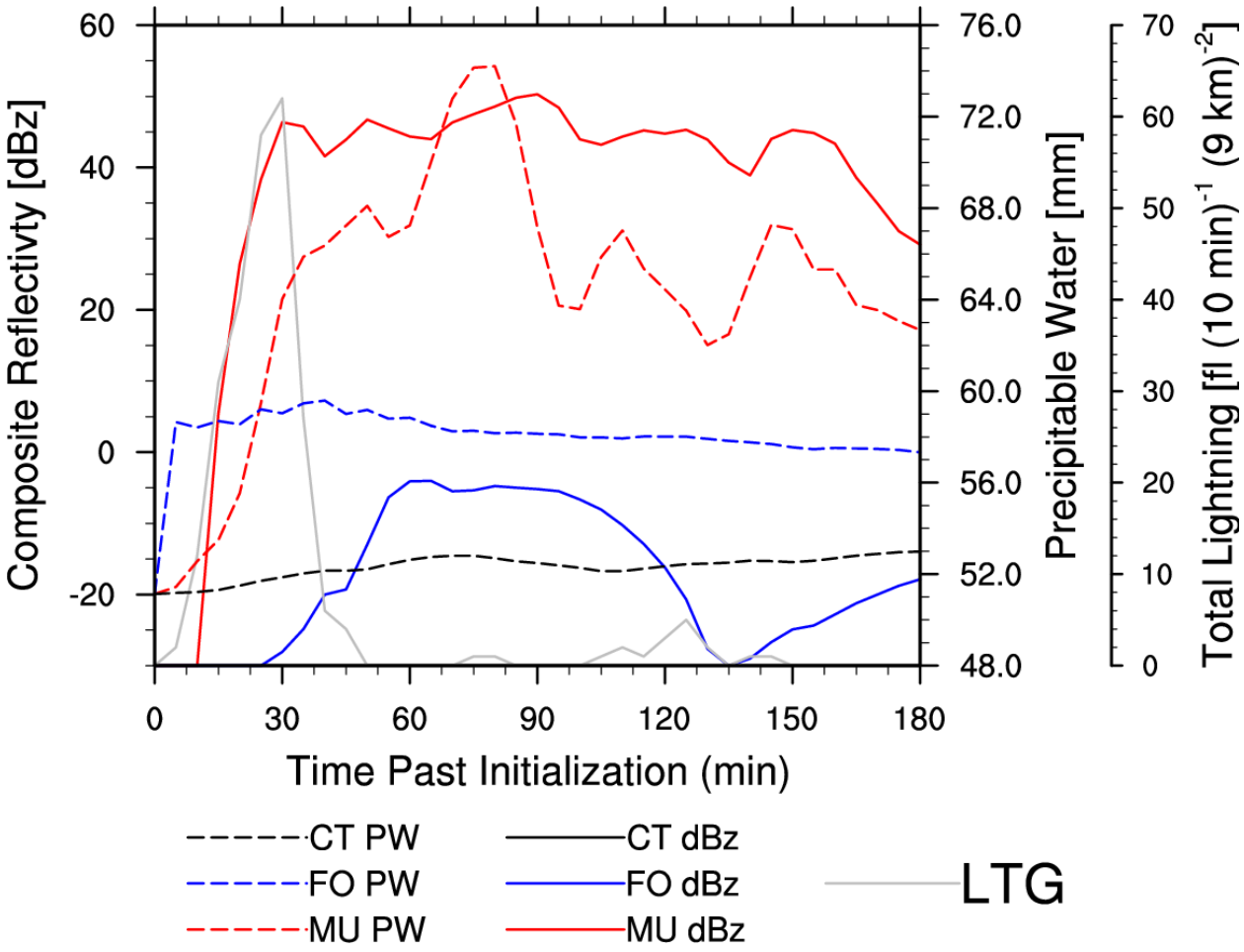

Fig. 7. Time series between 1200 UTC and 1500 UTC 9 June 2011 of observed total lightning (fl (10 min)$^{-1}$ (9 km)$^{-2}$, grey solid line), simulated composite reflectivity (dBz, solid lines), and simulated precipitable water (mm, dashed lines) for CT, MU, and FO using the same line colors and location as Figs. 4-6.

Compared to the MU simulation, convection in FO is slow to develop at the location of the observed storm in Figs. 4-6 that is nonexistent in the CT simulation. Figure 6 indicates some increase in relative humidity in the FO simulation, but the dry air below the freezing level and the absence of other forcing prevents deep convection from occurring. The evolution of simulated composite reflectivity in FO shows only negative dBz values occurring at the grid cell (blue solid line in Fig. 7). These values indicate that only clouds are occurring near the time of observed peak lightning activity (grey solid line). Meanwhile, MU produces clouds after 15 min of assimilation that initially are represented by small composite reflectivity (solid red line) but increase to significant values of ~ 45 dBz after 30 min of assimilation, indicative of deep

precipitating convection. The sharp increase in precipitable water (PW) after the start of assimilation illustrates the direct effects of the FO method (dashed blue line). However, indirect effects of the MU method also substantially increase PW (red dashed line). As updrafts begin to form in MU, PW increases slightly during the first 15 min of assimilation, but then increases by ~ 15 mm shortly afterward when low-level CAPE is accessed and a saturated adiabatic profile is realized up to ~ 500 hPa (Fig. 6). The storm in the MU simulation persists during the next 3 h which corresponds well with observed lightning.

Although the FO method often initiates precipitating convection, its failure to force deep convection in the stationary storm example (Figs. 4-7) is not a rare occurrence. As will be evident in later sections, FO is ineffective at some times and in certain regions. Sometimes its convection is relatively strong, with graupel mixing ratios of 1.0 g kg^{-1} or greater, but precipitation still does not occur at the surface. With no low-level updraft being induced, the area between convective cloud base and the mixed phase region remains too dry (as in Fig. 6 denoted by blue lines). If other forcing causes the atmosphere below the mixed phase region to be conducive to low-level convection, then FO becomes effective at initiating deep convection.

3.2 Systematic Effects of Lightning Assimilation Methods

The two lightning assimilation methods produce substantial effects on simulated fields of precipitation, temperature, and water vapor during all three severe storm cases. Since the methods only directly work in one direction, i.e., to enhance convection but not suppress it, large systematic biases in the model fields may degrade the usefulness of the resulting forecasts. A consideration of these biases puts the simulation results in a better context. The simulations employ a 12 h assimilation period ending at 0000 UTC, followed by a 12 h forecast period. Evaluating the subsequent forecast period without assimilation provides a better assessment of how the assimilation methods interact with the underlying model and how they may perform in an operational setting.

Hourly precipitation from MU and FO is greater than from CT on all three days (Fig. 8) when averaged over the verification domain (Fig. 1) during the assimilation period. After the assimilation period ends, the overprediction of precipitation relative to CT typically lasts only a few hours. The assimilation methods then often underpredict precipitation. This generalization is particularly apparent when one of the methods greatly overpredicts precipitation during the

assimilation period, such as the FO method on 27 April (Fig. 8a) and the MU method on 9 June (Fig. 8b). In all three cases the average precipitation of the CT simulation closely matches the stage IV (ST4) observations. No bias is noticeable in the CT simulation, except for two clear exceptions. The CT simulation overpredicts precipitation by ~ 50 % relative to ST4 during the first few hours of the 27 April case, when the model appears to still be spinning up. Conversely, CT underpredicts precipitation by ~ 50 % during the last 6 h of the 15 June case (Fig. 8c). During these periods both assimilation schemes do not mitigate the bias in the CT simulation. Given the precipitation biases of the assimilation schemes noted above, if the underprediction (overprediction) bias in the CT had occurred during (after) the assimilation period, assimilation would have assuaged the biased simulations of precipitation.

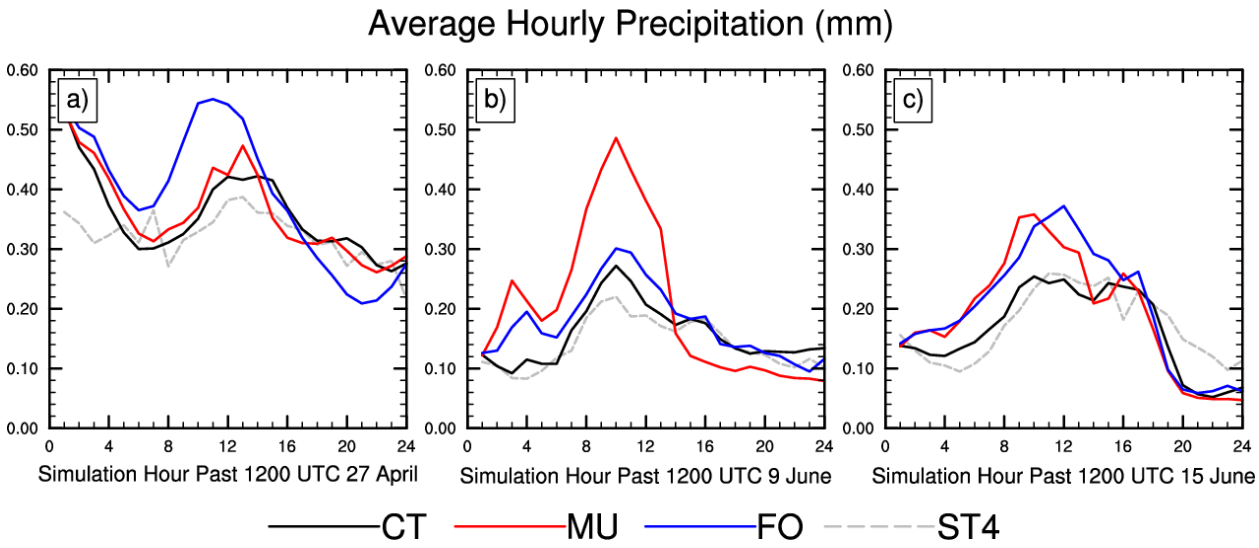

Fig. 8. Time series of hourly precipitation (mm) averaged over the verification domain (Fig. 1) for the first through last simulation hours on 27 April (a), 9 June (b), and 15 June 2011 (c) for the CT simulation (black line), MU simulation (red line), FO simulation (blue line), and stage IV observations (ST4; grey dashed line). The assimilation ends at 12 h past 1200 UTC.

Warming the model's temperature profile to initiate updrafts may create unrealistically strong updrafts. We assessed the maximum value of vertical velocity for the three-dimensional 3 km domain (i.e., considering all horizontal and vertical grid points) at each hourly simulation output time (Fig. 9). MU does not exhibit excessively greater values than the other simulations. While values from FO and CT closely match each other, the MU values are only ~ 25-50% greater and only during specific, seemingly random times during the assimilation period. We also averaged temperature for the three-dimensional 3 km domain. This allows us to conclude

that the MU and FO simulations exhibit consistently warmer values than CT on all three days, although sometimes only slightly warmer (Fig. 10). The greatest average temperature difference between MU and CT on 27 April, 9 June, and 15 June is, respectively, ~ 0.06 K, 0.13 K, and 0.08 K. These values are less than the diurnal range that is apparent in the figure. The MU simulation is consistently warmer than FO on 9 June and 15 June, but the average temperature of FO is similar to that of MU and often slightly warmer on 27 April.

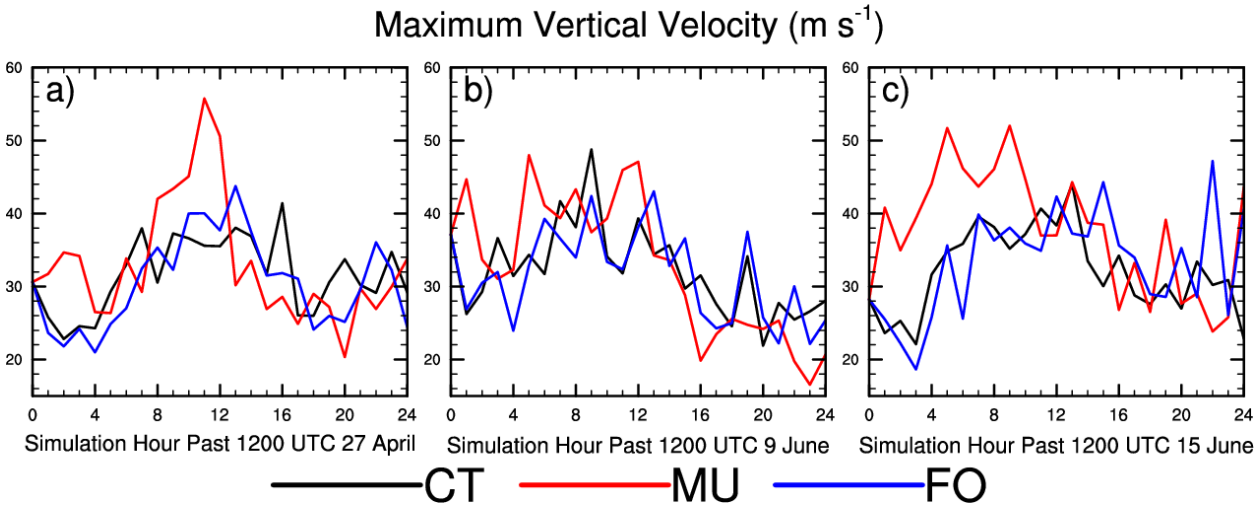

Fig. 9. As in Fig. 8, except instantaneous maximum vertical velocity (m s^{-1}) in the entire 3 km domain.

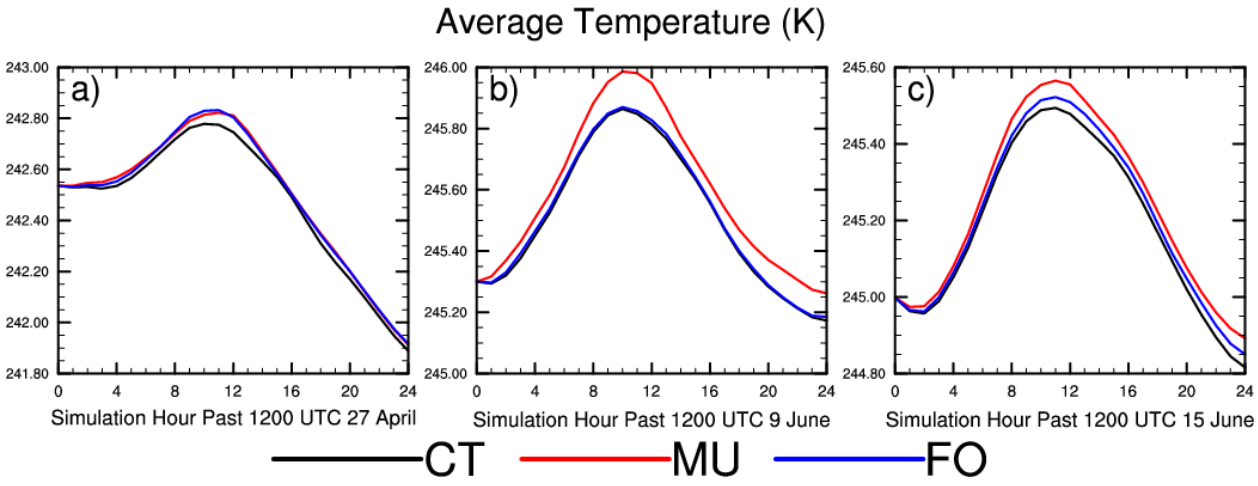

Fig. 10. As in Fig. 8, except temperature (K) averaged for the entire 3 km domain. Note that the panels have different scales on the y-axis.

The FO method does not directly alter temperature, but instead increases water vapor mixing ratios. Nonetheless, slightly warmer FO temperatures than MU do occur during the 27

April case (Fig. 10). The FO simulation consistently exhibits greater average PW than CT (Fig. 11). This increase in moisture by FO is ~ 0.3 mm, 0.8 mm, 0.4 mm, respectively, on 27 April, 9 June, and 15 June. By adding moisture to the model and producing more precipitation (as seen in Fig. 8), the additional latent heat release produces warmer average temperature relative to the CT. Merely adding moisture to the model does not cause warmer temperature. Instead, the added moisture must condense to produce latent heating. The PW of the FO simulation is greatest relative to CT on 9 June; however, the average temperature from FO is only slightly warmer than from CT. This modest increase in temperature results from the limited depletion of the water vapor added to the model by the FO method. The depletion of the water vapor via condensation and precipitation is modest since the average FO precipitation is only ~ 15% greater than CT (Fig. 8b).

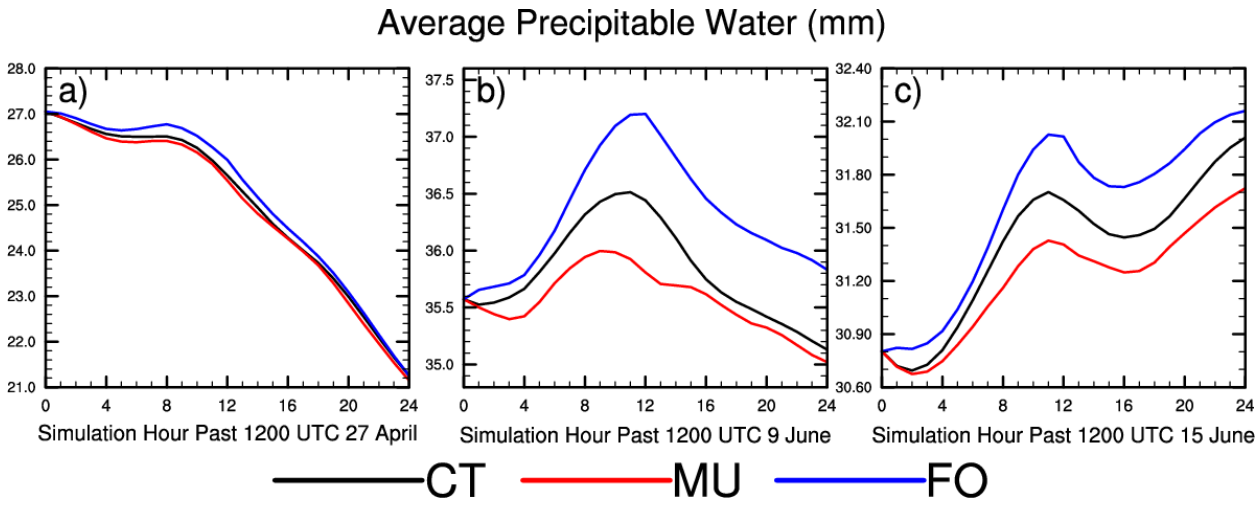

Fig. 11. As in Fig. 8, except precipitable water (mm) over the entire 3 km domain. Note that the panels have different scales on the y-axis.

Although the FO method has difficulty producing convection on 9 June, MU produces considerably more convection relative to CT. During one of the assimilation hours on 9 June, MU produces ~ 60% more precipitation than does CT (Fig. 8b). Without adding moisture to initiate convection, these far greater precipitation amounts produce a much drier atmosphere during the MU simulation than during CT (Fig. 11b). During the 27 April case, MU exhibits only slightly more average precipitation than does CT, while FO produces far greater rainfall amounts. On this day the MU method operates ineffectively, because large sheared storm anvils with qgmax exceeding 1.0 g kg^{-1} are produced in Mississippi and Alabama (not shown).

3.3 Subjective Verification of Simulated Precipitation Fields

A visual comparison between simulated (MU and FO) and observed (ST4) hourly precipitation fields from the lightning assimilation methods illustrates their performance and characteristics. This comparison is most revealing at the last hour of the assimilation period ending at 0000 UTC (Figs. 12-14) when the assimilation results become a unique blend of the CT simulation and ST4 observations. In addition, considering accumulations during the 0500-0600 UTC interval (Fig. 15) illustrates how quickly the assimilation can be forgotten, with the simulations returning to the CT solution. This section is followed by a statistical comparison of the simulations with observations.

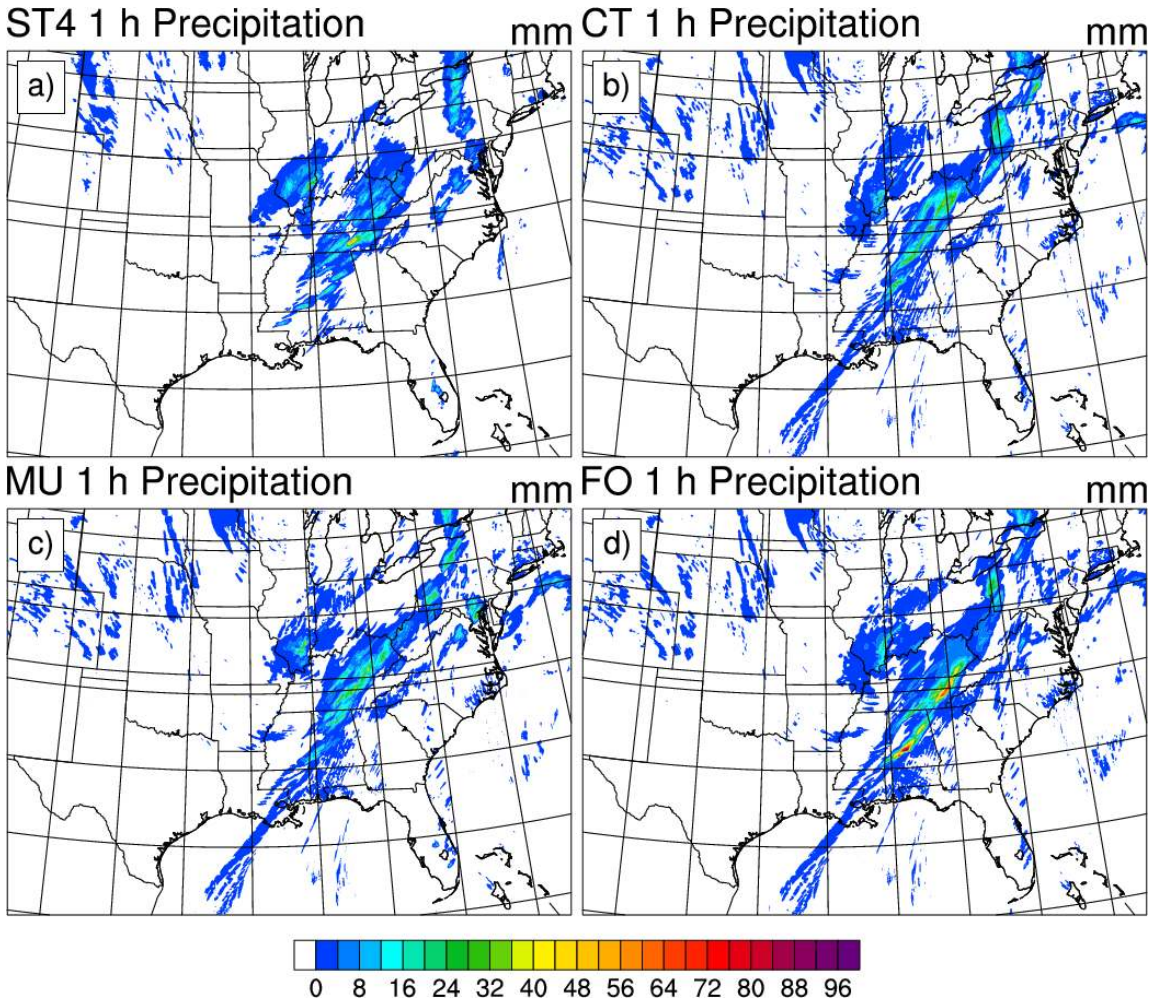

Fig. 12. Comparison of 1 h precipitation accumulation (mm) between 2300 UTC 27 April and 0000 UTC 28 April 2011 for (a) observed (ST4) and simulated sources: (b) CT, (c) MU, and (d) FO.

The pattern of 1-h accumulated precipitation is similar for all three simulations (CT, MU, and FO) of the 27 April case (Fig. 12); however, each exhibits slight differences compared with ST4. The simulations produce rain areas that are somewhat too large in Alabama and Mississippi, evidence of the inability to capture the true supercell nature of the observed storms at even 3 km grid spacing. FO produces a small area of very heavy rainfall (~80 mm) in central Alabama compared to the ST4 value of only ~ 20 mm. Conversely, CT and MU exhibit only small rainfall amounts in this location. The MU simulation better reproduces the observed large rainfall amounts near Washington, D.C. and an isolated convective cell in central Florida.

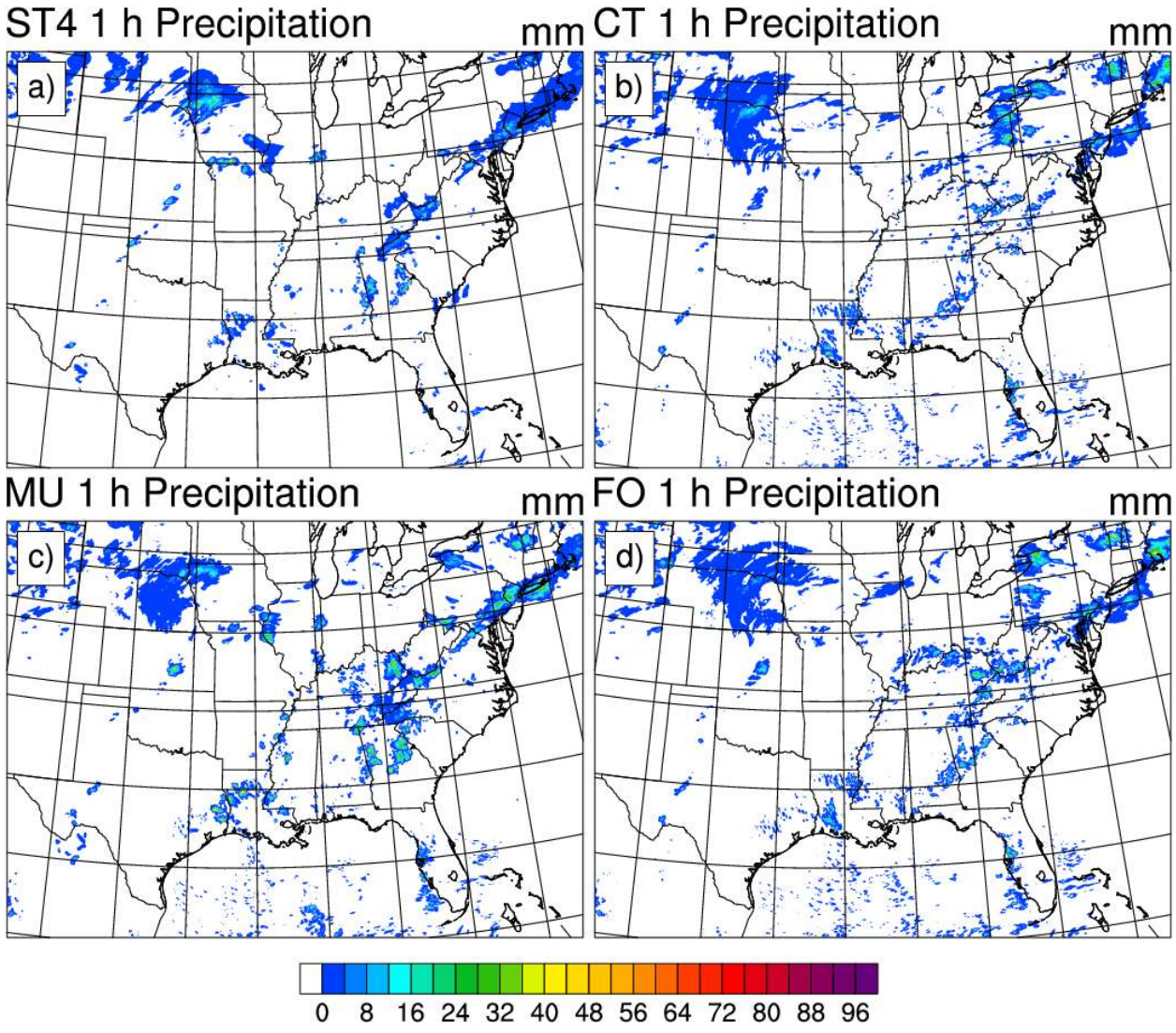

Fig. 13. As in Fig. 12, except between 2300 UTC 9 June and 0000 UTC 10 June 2011.

The MU simulation properly locates convection on 9 June across the Southeast and Northeast (Fig. 13), but the precipitation amounts are too large. Compared to MU and CT, FO best simulates precipitation amounts across the Southeast; however, there are numerous displacement errors. FO exhibits few differences from CT, which also was evident when examining the domain averaged precipitation (Fig. 8b). Although FO's precipitation fields are similar to those of CT, the FO simulation produces larger totals in areas such as Georgia, Kansas, and southeastern Pennsylvania. The utility of the FO method is particularly noticeable by its simulation of a convective line in Kansas. The CT simulation produces these storms in the proper locations, but its rainfall totals are too weak. Along with MU, FO produces precipitation amounts closer to those observed by ST4. MU generally on 9 June performs better than FO at correctly locating storms than FO given weakly forced thunderstorms across the Eastern United States.

Examining the representation of a spurious area of precipitation by the three simulations provides insight into how sometimes the assimilation methods eliminate or diminish spurious convection. The spurious precipitation feature near eastern Ohio or western Pennsylvania on 9 June (Fig. 13) is distinct between the three simulations with MU eliminating the feature more than FO. FO displaces the spurious precipitation eastward relative to the CT and succeeds somewhat in eliminating it, although not as well as MU. The spurious precipitation is due to the simulated storms being erroneously located too far west at the start of assimilation (not shown). Both assimilation methods properly place the convection farther east as the storms propagate eastward into Indiana and Ohio. However, after the observed precipitation dissipates at ~ 1800 UTC, both MU and FO continue to propagate the erroneous convection. MU's spurious precipitation mostly dissipates by 2300 UTC, but persists a few additional hours in FO. By correctly producing stronger convection farther east than CT near the start of assimilation, MU and FO diminish the spurious precipitation near the end of assimilation.

The simulations on the 15 June case produce the same general precipitation features as are observed with no large regions of significant spurious precipitation amounts (Fig. 14), but for some of the features the placement and orientation are distinct between simulations. For instance, the area of intense rainfall accumulations near southeastern Tennessee is too large in the MU simulation, but is better located than in CT and FO. MU also captures the void between precipitation features in far northern Georgia. MU and FO produce a precipitation area at the proper location and intensity in western Kansas that CT depicts poorly. FO likely succeeds in

simulating the Kansas convection because forcing already is present, as indicated by the weak CT convection in the same general area. FO produces more favorable environmental conditions at the locations of observed lightning and then properly simulates the approximate placement and amount of precipitation. Similarly, MU initiates updrafts through low-level warming that eradicate any inhibition where lightning is observed and allows deep convection appropriate for the simulated environment.

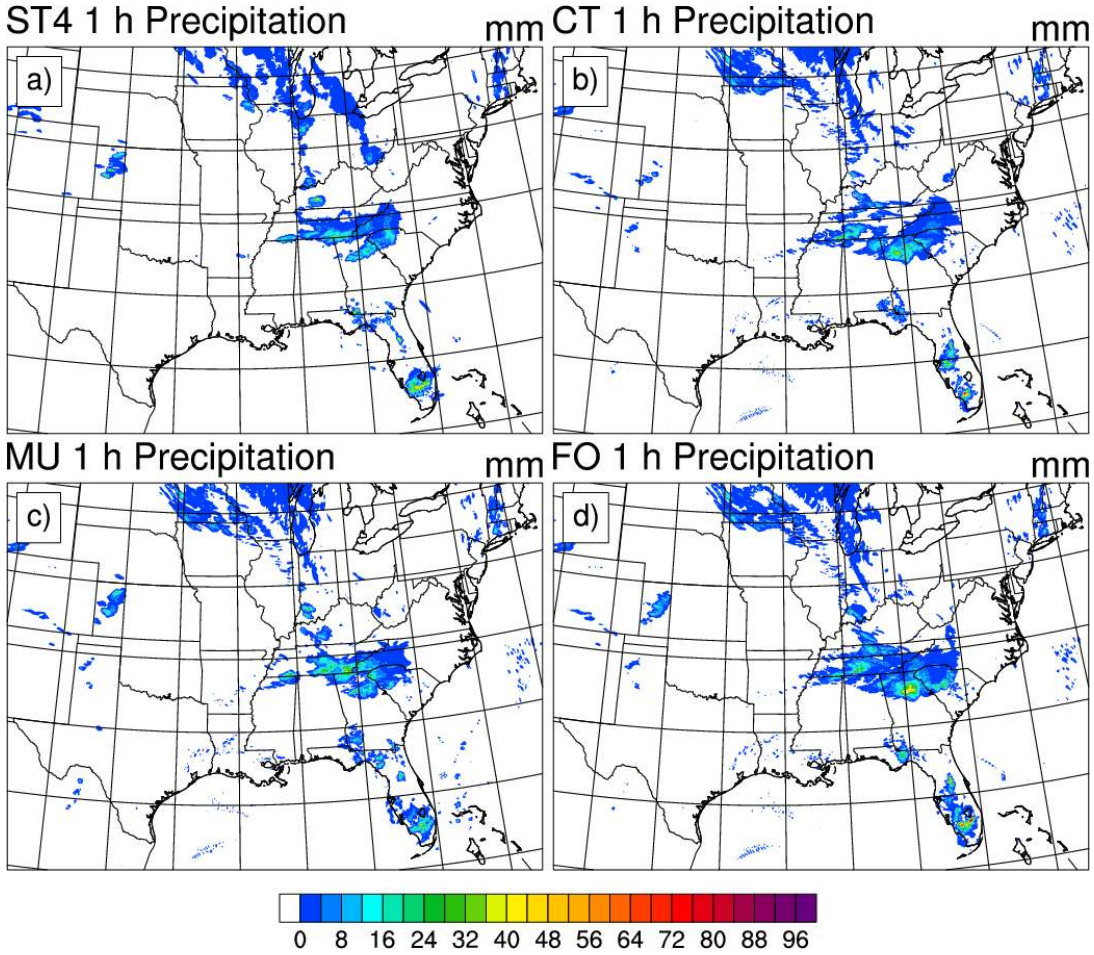

Fig. 14. As in Fig. 12, except between 2300 UTC 15 June and 0000 UTC 16 June 2011.

We next examine the sixth forecast hour after the end of the 12 h assimilation period (between 0500 - 0600 UTC 16 June) (Fig. 15) when only one precipitation feature near Georgia is apparent. MU and FO better maintain the integrity of this feature compared to CT. However, MU and FO poorly locate the area of intense rainfall just offshore of Georgia. Figure 15

illustrates that areas of large rainfall amounts are often sparse between 0300 and 1200 UTC. With few areas of rainfall the improvements from the assimilation methods are indiscernible.

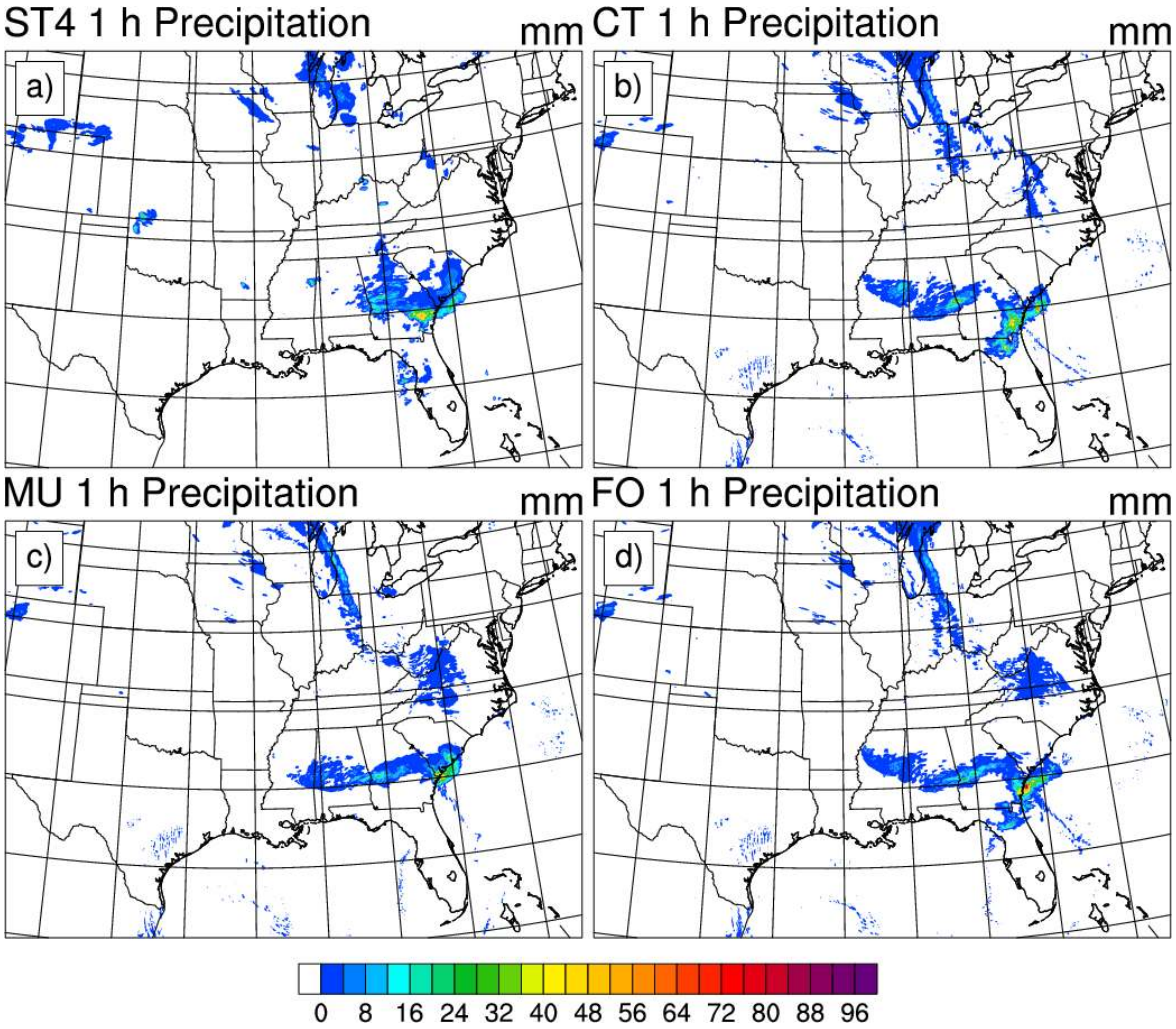

Fig. 15. As in Fig. 12, except 6 h after the end of the assimilation period, i.e., between 0500 UTC 16 June – 0600 UTC 16 June 2011.

3.4 Objective Hourly Precipitation Scores

The simulations can be evaluated quantitatively with the ST4 observations by computing objective precipitation scores for each hour, case, and using three precipitation thresholds (1, 5, and 10 mm). Along with the simulations using the 12 h assimilation period between 1200 UTC and 0000 UTC that we have been describing, we also compute hourly precipitation scores for simulations using the MU and FO methods for the complete 24 h period ending at 1200 UTC

(MU24 and FO24, respectively). Including these runs will illustrate that the results are improved if assimilation continues.

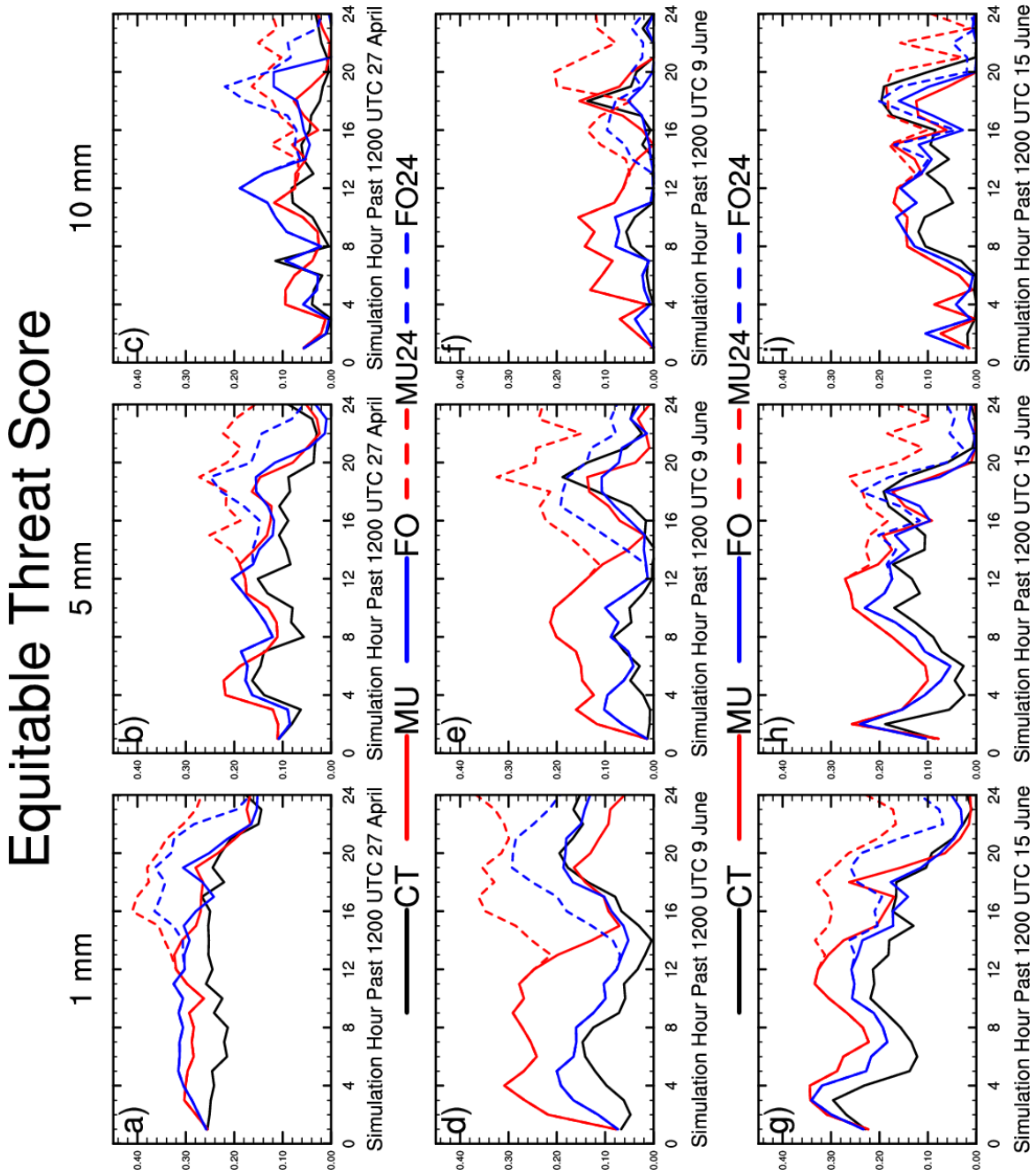

Fig. 16. Time series of hourly precipitation equitable threat score (ETS) relative to ST4 observations for five different simulations (CT in black, MU in solid red, FO in solid black, MU24 in dashed red, FO24 in dashed blue) and for three severe storm cases and three different precipitation thresholds: on 27 April for (a) 1 mm, (b) 5 mm, and (c) 10 mm threshold, on 9 June for (d) 1 mm, (e) 5 mm, and (f) 10 mm threshold, and on 15 June for (g) 1 mm, (h) 5 mm, and (i) 10 mm threshold. The assimilation ends at 12 h past 1200 UTC. The 6 h spin up period before 1200 UTC is not considered in the results.

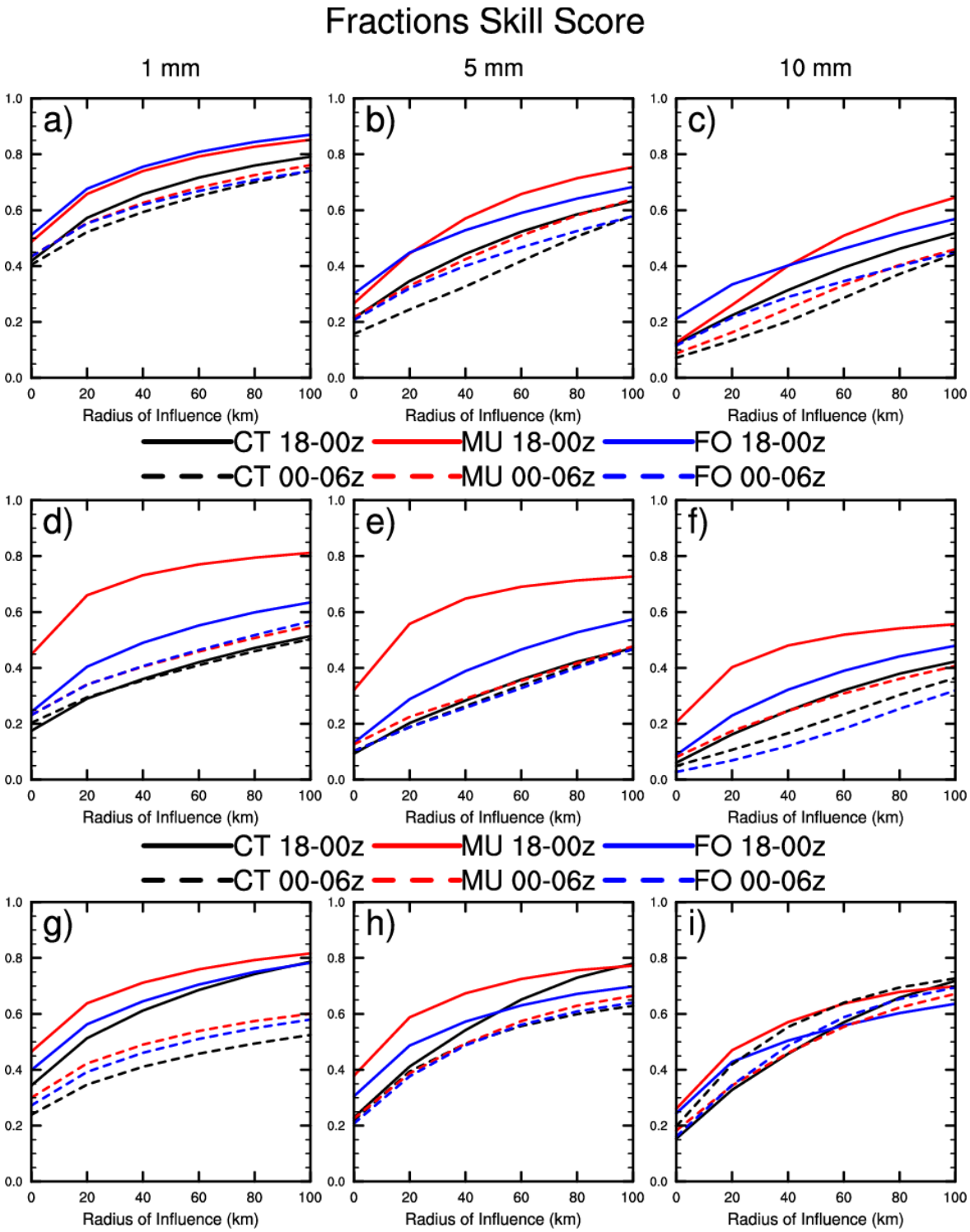

Fig. 17. Fractions skill score (FSS; y-axis) averaged over the last 6 h of the assimilation period (1800-0000 UTC, solid lines) and over the non-assimilation period (0000-1200 UTC, dashed lines) using six radii of influence (km, x-axis) for three severe storm cases and three different thresholds: on 27 April for (a) 1 mm, (b) 5 mm, and (c) 10 mm threshold, on 9 June for (d) 1 mm, (e) 5 mm, and (f) 10 mm threshold, and on 15 June for (g) 1 mm, (h) 5 mm, and (i) 10 mm threshold.

Certain generalizations about the ETS (Fig. 16) and FSS (Fig. 17) of the simulations are applicable on all three study days. MU and FO perform better than CT in terms of greater ETS and FSS during the assimilation period for all three precipitation thresholds. After the 12 h assimilation period, MU and FO generally perform better than CT in terms of ETS during the simulations hours 13 through 18 past 1200 UTC of the respective days. This improvement is more evident for the 1 mm and 5 mm thresholds than the 10 mm threshold since the latter occupy less area and are more prone to displacement errors. The improvement wanes with time, and no assimilation method exhibits clear improvement between simulation hours 19-24.

MU produces consistently greater ETS and FSS scores than FO during the assimilation period on 9 June (Figs. 16d-f and solid lines of Figs. 17d-f). MU also scores better during the assimilation period on 15 June at both the 1 mm and 5 mm thresholds, while scores are similar at the 10 mm threshold. During 27 April when MU has difficulty forcing additional deep convection, FO typically performs slightly better than MU in terms of ETS. When assessing FSS during the last six hours of assimilation (ending with simulation hour 12), MU actually scores better than FO for the 5 and 10 mm thresholds at the larger radii of influence (x-axis of Fig. 17). One should recall from section 2.6 of the methodology that larger radii are not as likely to penalize large displacement errors. When the assimilation continues past simulation hour 12 (dashed lines of Fig. 16), the MU24 simulation performs better and exhibits consistently greater ETS than the FO24 simulation for the 1 mm and 5 mm thresholds. For the 10 mm threshold, ETS become more ambiguous during the 27 April and 15 June cases.

The frequency bias (BIA) of the MU and FO simulations relative to CT indicates a deficiency of both assimilation methods (Fig. 18). The CT simulation initiated with the FNL data typically has a BIA near 1.0 at all three precipitation thresholds, indicating little bias relative to the ST4 observations. As expected, the simulations using assimilation to force convection usually exhibit BIA greater than 1.0 during the assimilation period. For example, BIA for the 5 and 10 mm thresholds can exceed 2.0 for MU and FO. When BIA exceeds 2.0, the simulated area exceeding the threshold is greater than twice the size of the area actually observed. After the assimilation period, MU often exhibits a BIA less than that of the CT simulation, likely due to atmospheric stabilization after the excessive convective precipitation during the assimilation period. When the assimilation continues after the 12th simulation hour, the large BIA diminishes

for MU24 and FO24 (dashed lines of Fig. 18), although it still is consistently greater than that of CT.

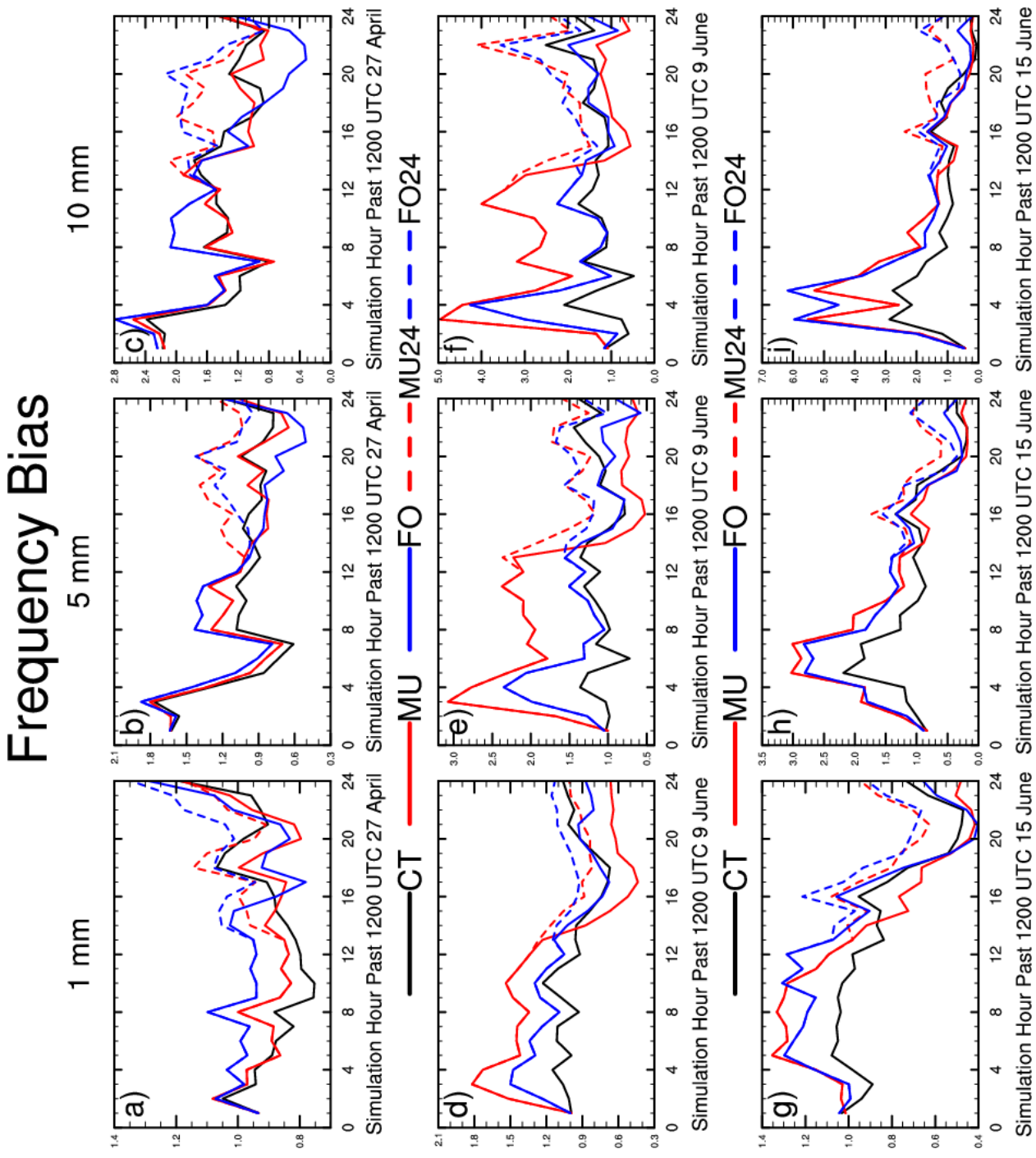

Fig. 18. As in Fig. 16, except for frequency bias (BIA). Note that the panels have different scales on the y-axis.

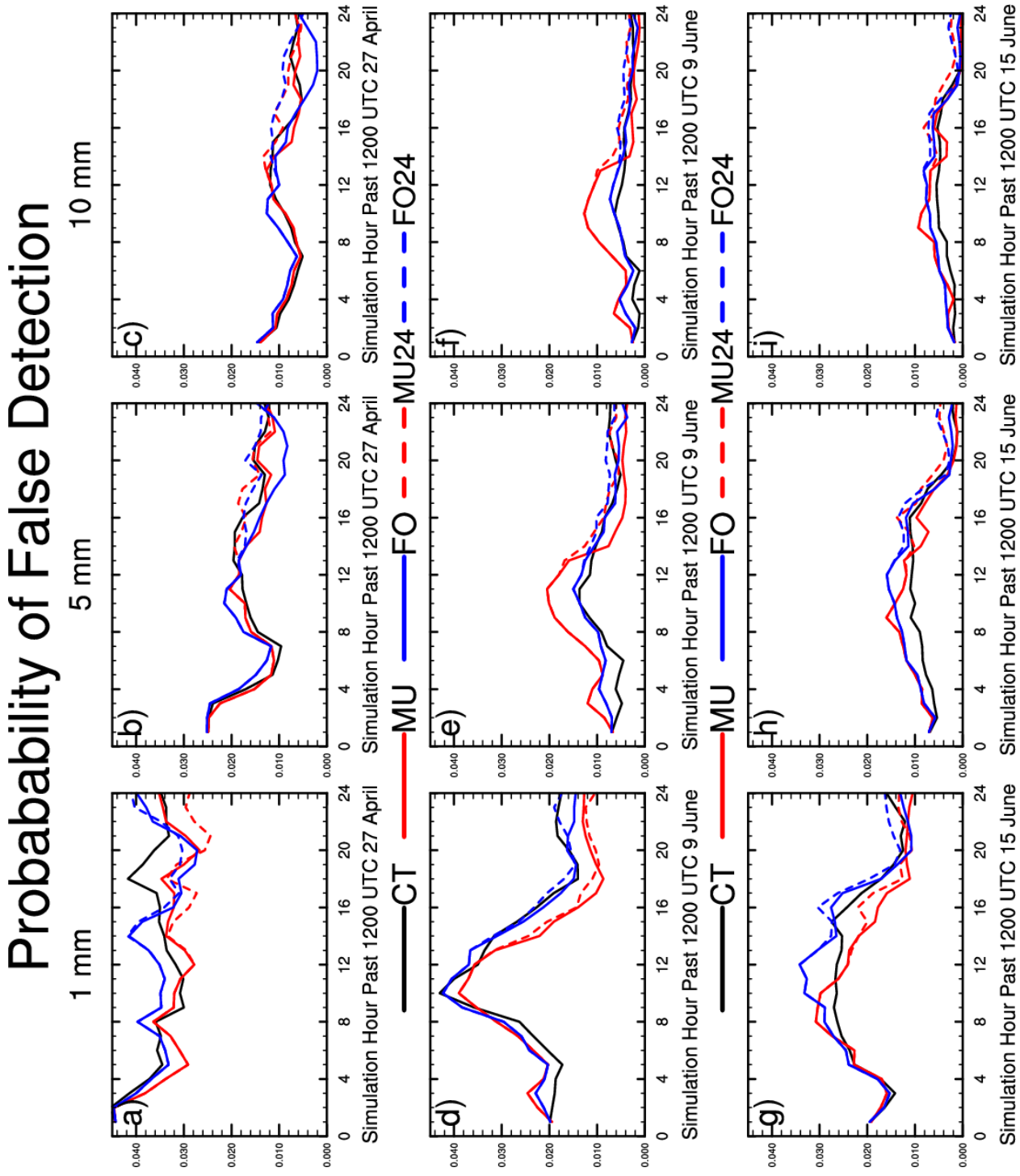

Fig. 19. As in Fig. 16, except for probability of false detection (POFD).

The probability of false detection (POFD) is a metric that indicates bias and the degree of agreement between locations of simulated and observed precipitation. A small value indicates

that a simulation is not falsely producing many areas that exceed the threshold. Employing an overly active and biased lightning data assimilation method would produce a greater POFD relative to the CT simulation. At the 5 mm and 10 mm thresholds, the POFD of MU and FO is indeed consistently greater than that of CT during assimilation (Fig. 19). When considering the 1 mm threshold, however, the POFD is sometimes less for FO and MU than CT, even during assimilation. At this small 1 mm threshold, the MU simulations generally have a POFD less than that of FO. The smaller POFD in MU can result from the MU method better locating a storm early in its life cycle and properly propagating the storm as previously discussed in section 3.3 for the 9 June case.

CHAPTER FOUR

SUMMARY AND CONCLUSIONS

A new nudging method has been developed to assimilate lightning data into numerical models. The nudging method (denoted MU) warms the most unstable low levels of the simulated atmosphere in locations where lightning is observed but not simulated as diagnosed by the presence of graupel exceeding 1.0 g kg^{-1}. The objective is to initiate updrafts and deep convection in those locations. Observed total lightning data for method development were from the Earth Networks System. The data were binned into 9×9 km grid cells to approximate what will be detected by the upcoming GOES-R lightning mapper. Simulations were performed across the Central and Eastern United States during three of the most electrically active days of 2011 in the simulated region.

Results show that the MU method is a viable alternative to the relative humidity nudging method (FO method) developed by Fierro et al. (2012) for assimilating lightning at cloud-resolving scales. Both the MU and FO methods improved simulated precipitation relative to control runs in which no assimilation was performed. This finding is based on equitable threat scores (ETS) and fraction skill scores using stage IV precipitation observations. These scores improved during assimilation and during a subsequent forecast period, but only out to approximately 6 h. For the two June cases, MU improved ETS of the 1 and 5 mm precipitation amounts during the last hour of the assimilation period by more than 0.1 relative to the control. ETS improvement was smaller for the 10 mm amount and 27 April case.

Although the FO method at times was more effective at producing correctly located and appropriate amounts of precipitation than MU, the MU method often proved more capable of producing deep convection in cases of observed isolated thunderstorms and storms with weak forcing. This increased effectiveness was a result of MU's ability to initiate an updraft in the low levels of the atmosphere that could force convection capable of accessing the environmental CAPE. In contrast, the FO method added moisture in the 0 to -20˚C mixed phase region. The added moisture, by increasing the virtual temperature, enhanced buoyancy, but the resulting updraft often was confined in the mid-levels. Since the added buoyancy from FO occurred in the mid-levels, sometimes the low levels near the convective cloud base would remain relatively dry. This dry layer would then prevent parcels from remaining saturated, accessing CAPE, and

eventually producing a thunderstorm. Although the greater humidity in the mid-levels made deep convection more likely, without low-level forcing the FO method often could not produce a thunderstorm where one was observed. This is a critical difference between MU and FO and often allows MU to perform considerably better than FO when the CT fails to produce precipitating convection in a region where lightning is observed.

The FO method's dependency on the intensity of the flash density is a strength in one aspect, but in another aspect it also may represent a limitation. In large areas of lightning occurrence as was common for the 27 April case, the humidity may increase more in the locations with more intense flash densities according to the nudging function, thereby favoring that location for intense updrafts and more precipitation. However, that added dependence means the nudging function is only appropriate for ENTLN observations and still may need to be updated as the detection efficiencies improve. Additionally, the nudging function would have to be recalibrated if using lightning data from another network including the future Geostationary Lightning Mapper. By assimilating the same way regardless of whether one or multiple flashes occur, the MU method is more exportable for different lightning networks.

Both the FO and MU assimilation methods operate at locations of observed lightning to produce or enhance convection but never act to suppress simulated convection where no lightning is observed. As a result, excessive areas and amounts of precipitation often occurred during assimilation. However, sometimes the procedures, particularly the MU method, indirectly suppressed the excessive precipitation by better locating storms early in their life cycle and properly propagating them to the correct locations. Nevertheless, the overprediction of precipitation still occurred, which may diminish the usefulness of both assimilation procedures for analysis purposes. This early overprediction, however, may be venial since a better forecast is the objective of the assimilation and the precipitation bias quickly disappears after the assimilation period. Nevertheless, the bias is a symptom of a larger issue with overprediction during assimilation. Specifically, a few hours into the forecast period after assimilation, precipitation often is underforecast relative to the control simulation. This occurs because the MU method warms the atmosphere to produce thunderstorms whose precipitation dries and stabilizes the atmosphere relative to the control. Conversely, the FO method moistens the atmosphere to produce thunderstorms, thereby warming and stabilizing the atmosphere. In contrast to the MU method's dry bias, the FO method produces a moist bias since a portion of

the added moisture remains in the atmosphere and fails to precipitate out. These effects of the assimilation may impair results during both the assimilation period and the subsequent forecast period, thereby preventing further improvements from the assimilation methods.

An assimilation method that directly suppresses convection in areas where lightning is not observed might diminish the current precipitation bias as well as moisture and temperature biases. However, developing such a method would be difficult since the absence of lightning does not preclude shallow warm rain convection from occurring. Therefore, one must formulate an assimilation method that only suppresses convection that extends above the freezing level. Furthermore, the absence of observed lightning at a location where it is simulated by the presence of graupel could indicate that either the atmosphere there is stable, or that the atmosphere is conditionally unstable and a trigger for deep convection has not yet occurred. Thus, the best way to suppress convection in these scenarios is unknown. Effectively suppressing and modulating convection would necessitate additional atmospheric observations and/or more sophisticated, computationally expensive methods of assimilation.

A potential low-cost solution to the moisture and temperature bias problem might concurrently employ a grid nudging method that weakly nudges the model's temperature, moisture, and wind fields to a high quality analysis. The grid nudging would occur at all grid points regardless of whether lightning was observed. It would occur simultaneously with the strong nudging performed by the warming MU method. In regions where lightning is observed but not simulated, the effects of the MU method would dominate those of the grid nudging. This concurrent method would diminish the temperature and moisture biases and potentially produce an improved analysis and ensuing forecast.

Further improvements in lightning data assimilation likely will require more sophisticated methods. For example, the MU method has the potential to be implemented within the EnKF or 4DVAR assimilation schemes. Mansell (2013) and Allen and Mansell (2013) indicated that EnKF can modulate deep convection by considering the intensity of observed lightning and the corresponding simulated graupel content. However, both EnKF and 4DVAR often have difficulty assimilating lightning where no storm exists and lightning proxies such as graupel mixing ratio are zero. A first guess field of zero simulated flashes produces a Jacobian of zero and no sensitivity to the observation (Evensen 2003, Errico et al. 2007). Consequently, these sophisticated methods are unable to modify the analysis at this location despite observations

clearly indicating that the analysis should be modified. Since the MU method has a demonstrated ability to initiate convection, it could be employed to produce convection in the first-guess fields when running the model forward. With a non-zero Jacobian, the sophisticated procedures could then successfully modulate convection.

It is hoped that weather forecasts will improve with the upcoming launch of GOES-R and its Geostationary Lightning Mapper (GLM). These forecast improvements will require the successful and effective assimilation of total lightning data. The GLM represents a potential source of valuable information about deep convection over the United States and regions of poor or no radar coverage. Our low-level warming nudging method serves as an effective and computationally inexpensive technique in which total lightning data can be assimilated into numerical weather models and thereby expand the utility of the GLM.

REFERENCES

Alexander, G. D., J. A. Weinman, V. Karyampudi, W. S. Olson, and A. C. L. Lee, 1999: The effect of assimilating rain rates derived from satellites and lightning on forecasts of the 1993 Superstorm. Mon. Wea. Rev., 127, 1433–1457.

Allen, B. J., and E. R. Mansell, 2013: Assimilation of pseudo Geostationary Lightning Mapper observations into a storm scale numerical model using the ensemble Kalman filter. 6th Conf. on the Meteorological Applications of Lightning Data, Austin, TX, Amer. Meteor. Soc., 7.1.

Anthes, R. A., 1974: Data assimilation and initialization of hurricane prediction model. J. Atmos. Sci., 31, 702–719.

Baldwin, M. E., J. S. Kain, and M. P. Kay, 2002: Properties of the convection scheme in NCEP's Eta Model that affect forecast sounding interpretation. Wea. Forecasting, 17, 1063–1079.

Baldwin, M. E., and J. S. Kain, 2006: Sensitivity of several performance measures to displacement error, bias, and event Frequency. Wea. Forecasting, 21, 636–648.

Barthe, C., and J.-P. Pinty, 2007: Simulation of a supercellular storm using a three-dimensional mesoscale model with an explicit lightning flash scheme. J. Geophys. Res., 112, D06210, doi:10.1029/2006JD007484.

Barthe, C., W. Deierling, and M. C. Barth, 2010: Estimation of total lightning from various storm parameters: A cloud-resolving model study. J. Geophys. Res., 115, D24202, doi:10.1029/2010JD014405.

Betts, A. K., 1986: A new convective adjustment scheme. Part I: Observational and theoretical basis. Quart. J. Roy. Meteor. Soc., 112, 677–692.

Betts, A. K., and M. J. Miller, 1986: A new convective adjustment scheme. Part II: Single column tests using GATE wave, BOMEX, and arctic air-mass data sets. Quart. J. Roy. Meteor. Soc., 112, 693–709.

Chagnon, J. M., and P. R. Bannon, 2005: Wave response during hydrostatic and geostrophic adjustment. Part I: Transient dynamics. J. Atmos. Sci., 62, 1311–1329.

Chang, D.-E., J. A. Weinman, C. A. Morales, and W. S. Olson, 2001: The effect of spaceborne microwave and ground-based continuous lightning measurements on forecasts of the 1998 Groundhog Day storm. Mon. Wea. Rev., 129, 1809–1833.

Chen, F., and J. Dudhia, 2001: Coupling an advanced land surface–hydrology model with the Penn State–NCAR MM5 modeling system. Part I: Model implementation and sensitivity. Mon. Wea. Rev., 129, 569–585.

Dowell, D. C., L. J. Wicker, and C. Snyder, 2011: Ensemble Kalman filter assimilation of radar observations of the 8 May 2003 Oklahoma City supercell: Influences of reflectivity observations on storm-scale analyses. Mon. Wea. Rev., 139, 272–294.

Dudhia, J., 1989: Numerical study of convection observed during the Winter Monsoon Experiment using a mesoscale two-dimensional model. J. Atmos. Sci., 46, 3077–3107.

Ek, M. B., K. E. Mitchell, Y. Lin, E. Rogers, P. Grunmann, V. Koren, G. Gayno, and J. D. Tarpley, 2003: Implementation of Noah land surface model advances in the National Centers for Environmental Prediction operational mesoscale Eta model. J. Geophys. Res., 108, 8851, doi:10.1029/2002JD003296.

Errico, R. M., P. Bauer, and J.-F. Mahfouf, 2007: Issues regarding the assimilation of cloud and precipitation data. J. Atmos. Sci., 64, 3785–3798.

Evensen, G., 2003: The Ensemble Kalman Filter: theoretical formulation and practical implementation. Ocean Dynamics, 53, 343–367.

Fierro, A. O., L. M. Leslie, E. R. Mansell, and J. M. Straka, 2008: Numerical simulations of the electrification and microphysics of the weakly electrified 9 February 1993 TOGA COARE squall line: Comparisons with observations. Mon. Wea. Rev., 136, 364–379.

Fierro, A. O., E. R. Mansell, C. L. Ziegler, and D. R. MacGorman, 2012: Application of a lightning data assimilation technique in the WRF-ARW model at cloud-resolving scales for the tornado outbreak of 24 May 2011. Mon. Wea. Rev., 140, 2609–2627.

Futyan, J. M., and A. D. Del Genio, 2007: Relationships between lightning and properties of convective cloud clusters. Geophys. Res. Lett., 34, L15705, doi:10.1029/2007GL030227.

Gallus, W. A., Jr., and M. Segal, 2001: Impact of improved initialization of mesoscale features on convective system rainfall in 10-km Eta simulations. Wea. Forecasting, 16, 680–696.

Gandin, L. S., and A. H. Murphy, 1992: Equitable Skill Scores for Categorical Forecasts. Mon. Wea. Rev., 120, 361–370.

Goodman, S. J., R. J. Blakeslee, W. J. Koshak, D. Mach, J. Bailey, D. Buechler, L. Carey, C. Schultz, M. Bateman, E. McCaul Jr., and G. Stano, 2013. The GOES-R Geostationary Lightning Mapper (GLM). Atm. Res., 124-125, 34-49.

Hamill, T. M., 1999: Hypothesis tests for evaluating numerical precipitation forecasts. Wea. Forecasting, 14, 155–167.

Hong, S.-Y., and J.-O. J. Lim, 2006: The WRF single-moment microphysics scheme (WSM6). J. Korean Meteor. Soc., 42, 129–151.

Hu, M., M. Xue, and K. Brewster, 2006: 3DVAR and cloud analysis with WSR-88D level-II data for the prediction of the Fort Worth, Texas, tornadic thunderstorms. Part I: Cloud analysis and its impact. Mon. Wea. Rev., 134, 675–698.

Iacono, M. J., E. J. Mlawer, S. A. Clough, and J.-J. Morcrette, 2000: Impact of an improved longwave radiation model, RRTM, on the energy budget and thermodynamic properties of the NCAR community climate model, CCM3. J. Geophys. Res., 105, 14 873-14 890.

Janjić, Z. I., 1994: The step-mountain eta coordinate model: Further developments of the convection, viscous sublayer, and turbulence closure schemes. Mon. Wea. Rev., 122, 927–945.

Jones, C. D., and B. Macpherson, 1997: A latent heat nudging scheme for the assimilation of precipitation data into an operational mesoscale model. Meteor. Appl., 4, 269–277.

Kain, J. S., and J. M. Fritsch, 1993: Convective parameterization for mesoscale models: The Kain–Fritsch scheme. The Representation of Cumulus Convection in Numerical Models, Meteor. Monogr., No. 46, Amer. Meteor. Soc., 165–170.

Kasahara, A., R. C. Balgovind, and B. B. Katz, 1988: Use of satellite radiometric imagery data for improvement in the analysis of divergent wind in the tropics. Mon. Wea. Rev., 116, 866–883.

Klemp, J. B., and R. B. Wilhelmson, 1978: The simulation of three-dimensional convective storm dynamics. J. Atmos. Sci., 35, 1070–1096.

Krishnamurti T. N., J. Xue, H. S. Bedi, K. Ingles, and O. Oosterhof, 1991: Physical initialization for numerical weather prediction over the tropics. Tellus, 43A, 53–81.

Kuhlman, K. M., C. L. Ziegler, E. R. Mansell, D. R. MacGorman, and J. M. Straka, 2006: Numerically simulated electrification and lightning of the 29 June 2000 STEPS supercell storm. Mon. Wea. Rev., 134, 2734–2757.

Lericos, T. P., H. E. Fuelberg, M. L. Weisman, and A. I. Watson, 2007: Numerical simulations of the effects of coastlines on the evolution of strong, long-lived squall lines. Mon. Wea. Rev., 135, 1710–1731.

Lin, Y., and K. E. Mitchell, 2005: The NCEP stage II/IV hourly precipitation analyses: Development and applications. Pre-prints, 19th Conf. on Hydrology, San Diego, CA, Amer. Meteor. Soc., 1.2. [Available online at http://ams.confex.com/ams/pdfpapers/83847.pdf.]

Loftus, A. M., D. B. Weber, and C. A. Doswell III, 2008: Parameterized mesoscale forcing mechanisms for initiating numerically simulated isolated multicellular convection. Mon. Wea. Rev., 136, 2408–2421.

Lopez, P., 2011: Direct 4D-Var assimilation of NCEP stage IV radar and gauge precipitation data at ECMWF. Mon. Wea. Rev., 139, 2098–2116.

Mahfouf, J.-F., P. Bauer, and V. Marécal, 2005: The assimilation of SSM/I and TMI rainfall rates in the ECMWF 4D-Var system. Quart. J. Roy. Meteor. Soc., 131, 437–458.

Manobianco J., S. Koch, V. M. Karyampudi, and A. J. Negri, 1994: The impact of assimilating satellite-derived precipitation rates on numerical simulations of the ERICA IOP 4 cyclone. Mon. Wea. Rev., 122, 341–365.

Mansell, E. R., D. R. MacGorman, C. L. Ziegler, and J. M. Straka, 2005: Charge structure and lightning sensitivity in a simulated multicell thunderstorm. J. Geophys. Res., 110, D12101, doi:10.1029/2004JD005287.

Mansell, E. R., C. L. Ziegler, and D. R. MacGorman, 2007: A lightning data assimilation technique for mesoscale forecast models. Mon. Wea. Rev., 135, 1732–1748.

Mansell, E. R., 2013: Ensemble assimilation of simulated total lightning flash rates. 6th Conf. on the Meteorological Applications of Lightning Data, Austin, TX, Amer. Meteor. Soc., 7.1.

Marecal V., and J.-F. Mahfouf, 2003: Experiments on 4DVAR assimilation of rainfall data using an incremental formulation. Quart. J. Roy. Meteor. Soc., 129, 3137-3160.

Markowski, P. M., and Y. P. Richardson, 2010: Mesoscale Meteorology in Midlatitudes. Wiley-Blackwell, 41-47.

McCaul, E.W., Jr., and C. Cohen, 2002: The impact on simulated storm structure and intensity of variations in the mixed layer and moist layer depths. Mon. Wea. Rev., 130, 1722–1748.

McCaul, E.W., Jr., S. J. Goodman, K. M. LaCasse, and D. J. Cecil, 2009: Forecasting lightning threat using cloud-resolving model simulations. Wea. Forecasting, 24, 709–729.

Mittermaier, M. P., and N. Roberts, 2010: Intercomparison of spatial forecast verification methods: Identifying skillful spatial scales using the Fractions Skill Score. Wea. Forecasting, 25, 343–354.

Mlawer, E. J., S. J. Taubman, P. D. Brown, M. J. Iacono, and S. A. Clough, 1997: Radiative transfer for inhomogeneous atmosphere: RRTM, a validated correlated-k model for the longwave. J. Geophys. Res., 102D, 16 663–16 682.

Naylor, J., and M. S. Gilmore, 2012: Convective initiation in an idealized cloud model using an updraft nudging technique. Mon. Wea. Rev., 140, 3699–3705.

Papadopoulos, A., T. G. Chronis, and E. N. Anagnostou, 2005: Improving convective precipitation forecasting through assimilation of regional lightning measurements in a mesoscale model. Mon. Wea. Rev., 133, 1961–1977.

Park, S. K., and D. Zupanski, 2003: Four-dimensional variational data assimilation for mesoscale and storm-scale applications. Meteorol. Atmos. Phys., 82, 173–208.

Pessi, A. T., and S. Businger, 2009: Relationships between lightning, precipitation, and hydrometeor characteristics over the North Pacific Ocean. J. Appl. Meteor. Climatol., 48, 833–848.

Pessi, A. T., and S. Businger, 2009: The impact of lightning data assimilation on a winter storm simulation over the North Pacific Ocean. Mon. Wea. Rev., 137, 3177–3195.

Price, C., and D. Rind, 1992: A simple lightning parameterization for calculating global lightning distributions. J. Geophys. Res., 97, 9919-9933, doi:10.1029/92JD00719.

Pickering, K. E., Y. Wang, W.-K. Tao, C. Price, and J.-F. Müller, 1998: Vertical distributions of lightning NOx for use in regional and global chemical transport models. J. Geophys. Res., 103(D23), 31 203–31 216, doi:10.1029/98JD02651.

Roberts, N. M., 2005: An investigation of the ability of a storm scale configuration of the Met Office NWP model to predict flood-producing rainfall. Met Office Tech. Rep. 455, 80 pp.

Roberts, N. M., and H. W. Lean, 2008: Scale-selective verification of rainfall accumulations from high-resolution forecasts of convective events. Mon. Wea. Rev., 136, 78–97.

Rogers, R. F., J. M. Fritsch, and W. C. Lambert, 2000: A simple technique for using radar data in the dynamic initialization of a mesoscale model. Mon. Wea. Rev., 128, 2560–2574.

Rudlosky, S. D., and H. E. Fuelberg, 2011: Seasonal, regional, and storm-scale variability of cloud-to-ground lightning characteristics in Florida. Mon. Wea. Rev., 139, 1826–1843.

Rudlosky, S. D., and H. E. Fuelberg, 2013: Documenting storm severity in the Mid-Atlantic region using lightning and radar information. Mon. Wea. Rev., doi:10.1175/MWR-D-12-00287.1, in press.

Saunders, C. P. R., 1993: A review of thunderstorm electrification processes. J. Appl. Meteor., 32, 642–655.

Schaefer, J. T., 1990: The critical success index as an indicator of warning skill. Wea. Forecasting, 5, 570–575.

Schultz, C. J., W. A. Petersen, and L. D. Carey, 2011: Lightning and severe weather: A comparison between total and cloud-to-ground lightning trends. Wea. Forecasting, 26, 744–755.

Schwartz, C. S., and Coauthors, 2009: Next-day convection-allowing WRF model guidance: A second look at 2-km versus 4-km grid spacing. Mon. Wea. Rev., 137, 3351–3372.

Skamarock, W. C., and J. B. Klemp, 2007: A time-split non-hydrostatic atmospheric model for research and NWP applications. J. Comp. Phys., 227, 3465–3485.

Stauffer, D. R., and N. L. Seaman, 1990: Use of four-dimensional data assimilation in a limited-area mesoscale model. Part I: Experiments with synoptic-scale data. Mon. Wea. Rev., 118, 1250–1277.

Takahashi, T., 1978: Riming electrification as a charge generation mechanism in thunderstorms. J. Atmos. Sci., 35, 1536–1548.

Tong, M., and M. Xue, 2005: Ensemble Kalman filter assimilation of Doppler radar data with a compressible nonhydrostatic model: OSS Experiments. Mon. Wea. Rev., 133, 1789–1807.

Vonnegut, B., 1963: Some facts and speculation concerning the origin and role of thunderstorm electricity. Severe Local Storms, Meteor. Monogr., No. 27, Amer. Meteor. Soc., 224–241.

Weisman, M. L., W. C. Skamarock, and J. B. Klemp, 1997: The resolution dependence of explicitly modeled convective systems. Mon. Wea. Rev., 125, 527–548.

Weisman, M. L., and R. J. Trapp, 2003: Low-level mesovortices within squall lines and bow echoes. Part I: Overview and dependence on environmental shear. Mon. Wea. Rev., 131, 2779–2803.

Weygandt, S. S., S. G. Benjamin, M. Hu, T. G. Smirnova, and J. M. Brown, 2008: Use of lightning data to enhance radar assimilation within the RUC and Rapid Refresh models. Preprints, 3rd Conf. on Met. App. of Lightning Data, New Orleans, LA, Amer. Meteor. Soc., 7.3. [Available online at http://ams.confex.com/ams/pdfpapers/134112.pdf.]

Wilks, D. S., 1995: Statistical Methods in the Atmospheric Sciences. Academic Press, 467 pp.

Xiao, Q., and J. Sun, 2007: Multiple-radar data assimilation and short-range quantitative precipitation forecasting of a squall line observed during IHOP_2002. Mon. Wea. Rev., 135, 3381–3404.

BIOGRAPHICAL SKETCH

Max Marchand grew up in Naples, FL. There the frequent occurrence of thunderstorms on summer days spawned in him an interest in weather. Many summer days, that otherwise were highlighted by reruns of *The Simpsons* and *Kids in the Hall*, were spent hoping and waiting for the excitement of a thunderstorm. From a young age he also had an infatuation with numbers and math. Consequently, the ubiquitous nature of numbers and math in meteorology further ingrained the interest in weather. This fascination in numbers and mathematics and their ability to describe the intricacies of a topic also lends him an interest in baseball and financial markets.

The fascination in weather led him to Florida State University where he earned a Bachelor of Science in Meteorology in 2010. By pursuing a Master of Science, Dr. Henry Fuelberg gave him the opportunity to satisfy both his interests of thunderstorms and mathematics with a math-intensive research topic of lightning data assimilation. Upon completion, Max will continue researching the atmospheric sciences.